

1 Oxygen optodes on oceanographic moorings: recommendations for
2 deployment and in-situ calibration

3 Una Kim Miller¹, Kristen E. Fogaren², Dariia Atamanchuk³, Clare Johnson⁴, Jannes Koelling^{5, 6},
4 Isabela Le Bras⁷, Margaret Lindeman⁸, Hiroki Nagao^{7, 9}, David P. Nicholson¹⁰,
5 Hilary Palevsky², Ellen Park^{9, 10}, Meg Yoder², Jaime Palter¹

6 ¹Graduate School of Oceanography, University of Rhode Island

7 ²Department of Earth and Environmental Sciences, Boston College

8 ³Department of Oceanography, Dalhousie University

9 ⁴Scottish Association for Marine Sciences

10 ⁵Cooperative Institute for Climate, Ocean, and Ecosystems Studies, University of Washington

11 ⁶NOAA Pacific Marine Environmental Laboratory

12 ⁷Department of Physical Oceanography, Woods Hole Oceanographic Institution

13 ⁸University of Southampton

14 ⁹MIT-WHOI Joint Program in Physical Oceanography

15 ¹⁰Department of Marine Chemistry and Geochemistry, Woods Hole Oceanographic Institution

16 **Abstract**

17 Increasing interest in optical oxygen sensors, or optodes, on oceanographic moorings reflects the
18 value of dissolved oxygen (DO) measurements in studies of physical and biogeochemical processes.
19 Optodes are well-suited for moored applications but require careful, multi-step calibrations in the
20 field to ensure data accuracy. Without a standardized set of protocols, this can act as a barrier for
21 science teams lacking expertise in optode data processing and calibration. Here, we provide a set of
22 recommendations for the deployment, in-situ calibration, and treatment of data from moored optodes,
23 developed from our experience working with a set of 60 optodes deployed as part of the Gases in
24 the Overturning and Horizontal circulation of the Subpolar North Atlantic Program (GOHSNAP).
25 In particular, we detail the correction of drift in moored optodes, which occurs in two forms: (i)
26 an irreversible, time-dependent drift that occurs during both optode storage and deployment and
27 (ii) a reversible and pressure- and time-dependent drift that is detectable in some optodes deployed
28 at depths greater than 1,000 m. The latter is virtually unidentified in the literature yet appears to
29 effect a low-bias on the order of 1 to 3 $\mu\text{mol kg}^{-1}$ per 1000 m depth in the form of an exponential
30 decay over the first days to months of deployment. Comparisons of our calibrated DO time series
31 against serendipitous mid-deployment conductivity-temperature-depth (CTD)-DO profiles, as well as
32 biogeochemical (BGC)-ARGO float profiles, suggest the protocols described here yield an accuracy
33 in optode-DO of $\sim 1\%$, or roughly 2.5 to 3 $\mu\text{mol kg}^{-1}$. We intend this paper to serve as both
34 documentation of the current best practices in the deployment of moored optodes as well as a guide
35 for science teams seeking to collect high-quality moored oxygen data, regardless of expertise.

34 1 Introduction

35 Dissolved oxygen (DO) concentrations reflect a number of important processes in the ocean, including
36 ventilation of saturated surface waters, biological activity, and changes in solubility due to temperature
37 (Lévy et al. 2022; Oschlies et al. 2018; Palter and Trossman 2018). Oxygen is essential to the health of
38 marine ecosystems: The ongoing and widespread decline in DO concentrations across the world's oceans
39 (Diaz and Rosenberg 2008; Ito et al. 2017; Lévy et al. 2022) poses a significant threat to organisms
40 already living near the edge of their metabolic oxygen demand (Cheung et al. 2013; Deutsch et al.
41 2015; Diaz and Rosenberg 2008). DO is also of interest in studies of ocean circulation, serving as a
42 complementary tracer to temperature and salinity (e.g., Dove et al. 2021; Stendardo and Gruber 2012;
43 Thomas and Joyce 2010; Wolf et al. 2018). For these reasons, measuring DO has become a priority in
44 oceanographic research, prompting interest in sustained, autonomous time series made possible by the
45 moored deployment of oxygen sensors (D. Atamanchuk et al. 2020; Emerson and Stump 2010; Emerson
46 et al. 2008; Koelling et al. 2022).

47 Optical oxygen sensors, called optodes, are more stable over time than the electro-chemical sensors
48 ("electrodes"; Clark et al., 1953; Wei et al., 2019) commonly incorporated into shipboard conductivity-
49 temperature-depth (CTD) packages, making them the preferred sensor for long-term deployments on
50 floats, gliders, and moorings. However, optodes are known to drift substantially from factory calibration
51 over their lifetime, requiring additional, periodic calibrations by the user. A growing body of literature
52 seeks to characterize the nature of optode drift (e.g., Bittig et al. 2015; Bittig and Körtzinger 2015; Bittig
53 et al. 2018b; Bushinsky and Emerson 2013; Bushinsky et al. 2016; D'Asaro and McNeil 2013; Johnson
54 et al. 2015; Ren et al. 2023), but its mechanisms are not fully understood (SeaBird Electronics 2023),
55 and no universal drift correction exists. Each optode must therefore be individually calibrated, following
56 protocols that vary depending on the mode of deployment and optode design. As moored optode
57 deployments are still uncommon relative to float- and glider-based deployments, no such standardized
58 procedures exist for moorings, which can act as a barrier to science teams without prior optode experience.
59 This paper responds to the need to document the current best practices for the deployment and in-situ
60 calibration of fixed-depth optodes on oceanographic moorings. It additionally aims to serve as a step-by-
61 step guide for science teams seeking to collect high-quality, moored oxygen measurements. By focusing
62 on moorings, we complement the existing general guide to the principles and applications of optodes in
63 Bittig et al. 2018b, which had a primary focus on profiling platforms such as Argo floats.

64 The protocols for acquiring and processing optode data (Figure 1) recommended in this paper
65 were developed from our experience working with 60 moored optodes deployed over a 2-year period
66 on sections of the Overturning in the Subpolar North Atlantic Program (OSNAP; Lozier et al. 2019)
67 mooring array at depths ranging from approximately 50 m to 3400 m. These optodes were deployed as
68 part of the Gases in the Overturning and Horizontal circulation of the Subpolar North Atlantic Program
69 (GOHSNAP) (Dariia Atamanchuk et al. 2021 and Figure 1 therein). The main body of the text provides
70 both a conceptual and practical understanding of these protocols, with actionable steps summarized in
71 a "quick-start" guide in Appendix A, a step-by-step list meant to be referenced by the user throughout
72 the pre-deployment, deployment, and post-deployment stages of data handling. Key terminology used in

the main-body text and quick-start guide is summarized in the glossary (Table 1). Section 2 orients the reader to the physical principles behind optode measurements and provides a basic understanding of optode data processing and drift that helps rationalize the many calibration steps that follow. Section 3 guides the reader through optode selection and necessary pre-cruise and shipboard preparations. Section 4 describes the collection and calibration of shipboard DO casts, termed CTD-DO, that crucially provide pre- and post-deployment calibration points for the optode-DO. The accuracy of the optode-DO time series therefore rests on the accuracy of the CTD-DO, and special care must be taken in the calibration of the latter using Winkler-titrations of discrete seawater samples, or “Winklers” (Langdon 2010; Winkler 1888), detailed in Appendix B. Section 5 describes the recommended protocols for the processing of optode data, from raw instrument output to final, calibrated DO time series. Section 6 discusses sources of uncertainty in the calibrated optode-DO time series and presents a validation of 11 calibrated DO time series against fortuitous mid-deployment Winkler-calibrated CTD-DO profiles, as well as available biogeochemical(BGC)-Argo float DO (BGC-Argo-DO) profiles. Section 7 outlines aspects of Findable, Accessible, Interoperable, and Reusable (FAIR; Wilkinson et al. 2016) data archiving as applied to moored applications. Lastly, Section 8 summarizes key concepts and steps introduced in the text.

2 Overview

The basic physical principles of oxygen sensing with optodes are helpful context for the protocols described in this paper and are briefly described here; readers interested in a deeper technical understanding are referred to Lakowicz 1999 and Bittig et al. 2018b. Optodes are based on the principle of luminescence quenching, which is the reduction of fluorescent intensity in the presence of a specified substance: in this case, oxygen. The optode repeatedly excites a luminescent substance, or “luminophore,” immobilized within a flexible, oxygen-permeable substrate, referred to as a sensing foil (see Figure 1 in Tengberg et al. 2006 for a diagram of optode parts). The intensity and lifetime of emitted light is “quenched” (reduced) in the presence of oxygen, which the optode registers as a phase shift between the modulated luminophore excitation and light emission signals (see Figure 2 in Bittig et al. 2018b for a conceptual illustration). This phase shift can be related to DO concentration ($[O_2]$) with a modified version of the classic Stern-Volmer relationship, (Uchida et al. 2008),

$$[O_2] = \frac{(\phi_0/\phi - 1)}{K_{sv}} S_{corr} P_{corr} \quad (1)$$

Here, ϕ_0 is the phase shift in the absence of oxygen, ϕ is the phase shift recorded by the optode, and K_{sv} is the Stern-Volmer constant. ϕ_0 and K_{sv} are calculated using in-situ temperature measurements and manufacturer-determined coefficients from a “multi-point” factory calibration, in which the response of the optode’s sensing foil to DO in a range of temperatures and DO concentrations is characterized (Bushinsky and Emerson 2013). This response, and therefore calculation of Equation 1 (later detailed in Section 5.1), is specific to each individual sensing-foil/optode. S_{corr} and P_{corr} are correction factors that compensate for the effects of salinity and pressure, respectively, on the phase equilibrium between

107 the sensing foil and DO in the ambient seawater. S_{corr} is calculated from in-situ salinity measurements
108 and manufacturer-determined coefficients. P_{corr} is calculated from in-situ pressure measurements and a
109 user-determined coefficient. Pressure, in particular, causes substantial error in measured DO (order 1-3
110 $\mu\text{mol kg}^{-1}$ per 1000 m) at depths of more than several hundred meters because of its compounding effects
111 on the optode's luminophore, DO activity within the sensing foil, and luminescence quenching (Bittig et al.
112 2018b). In Figure 2, this pressure-dependent bias is made apparent with data from a "cal-dip", a CTD
113 cast in which optodes are affixed to the ship's CTD profiler frame, providing simultaneous and co-located
114 optode-DO and CTD-DO profiles: the optode-DO profile without any pressure correction (i.e., P_{corr} ;
115 solid black line) exhibits increasing bias with depth relative to the Winkler-calibrated CTD-DO profile
116 (solid blue line). This depth-dependent bias is removed by application of P_{corr} , as seen in the corrected
117 profile (dotted blackline). Note that the application of P_{corr} does not remove the depth-*independent*
118 (constant) bias in the optode-DO profile relative to the Winkler-calibrated CTD-DO profile, which arises
119 due to instrument drift and is handled in a separate step, described below and in Section 5.3).

120 The user must be aware of two types of time-dependent optode drift in the context of moored
121 deployments, one irreversible in nature and the other reversible. The "irreversible drift", so-called here
122 because its effects stay with the optode for its lifetime (i.e., do not reverse), has been widely observed in
123 float-based optode deployments (Bittig and Körtzinger 2017; Bittig et al. 2018b; Bushinsky et al. 2016;
124 D'Asaro and McNeil 2013; Johnson et al. 2015; Ren et al. 2023) and manifests in virtually all optodes as
125 a negative bias in measured DO. This negative bias has been shown to decay exponentially with time,
126 such that the most rapid drift occurs within several years of initial factory calibration and older optodes
127 can generally be considered more stable (Bittig et al. 2018b; D'Asaro and McNeil 2013; Ren et al. 2023).
128 The time-dependence of irreversible drift is augmented by sampling intensity, which is why manufacturers
129 subject optodes to extensive sampling ("burn-in" or "pre-maturation") prior to factory calibration in
130 order to reduce the magnitude of lifetime drift seen by the user (Bittig et al. 2018b). While irreversible
131 drift changes exponentially over the lifetime of the optode, the years-long time scale of its exponential
132 character results in in-situ drift appearing in moored time series as a quasi-linear decrease in optode-DO
133 (e.g., Figure 3a).

134 The "reversible" drift is also exponential in nature, though its characteristic exponential decay
135 occurs on a much shorter time scale, making it readily evident in uncalibrated moored optode-DO time
136 series (e.g., Figure 3b). The reversible drift is both pressure- and time-dependent, increasing with pressure
137 (depth) and occurring on time scales of days to months (Berx et al. 2019). The defining characteristic
138 of reversible drift is that, unlike irreversible drift, its effects reverse once the optode is recovered to the
139 surface. It can, therefore, only be quantified in-situ before the optode is recovered from the depth at
140 which it was deployed (*ibid.*). Its cause is unknown, but its dependence on pressure suggests that it may
141 be a time-dependent expression of the same mechanisms causing the instantaneous pressure-induced bias
142 seen in Figure 2 and corrected for with P_{corr} . We found that reversible drift was detectable in some, but
143 not all, of the moored GOHSNAP optodes deployed at depths of greater than 1000 m (further discussed
144 in Section 5.2).

145 The recommended calibration procedure for moored optode drift involves, first, removing reversible

146 drift, if present, by fitting and subtracting an exponential function of the form $y = ae^{-bx} + c$ to the
147 trace of the drift (Section 5.2). Next, irreversible drift is corrected for by applying a time-dependent gain
148 correction factor, $G(t)$, to the uncalibrated DO measurements,

$$[O_2]_{calibrated} = G(t)[O_2] \quad (2)$$

149 Here, $G(t)$ is a linear function fitted to two or more calibration points in time, e.g., $G(t_1)$ and $G(t_2)$,
150 calculated via comparison with shipboard CTD-DO collected upon mooring deployment and recovery
151 (See Figure 4 and Sections 4.1 and 5.3). Some forms of Equation 2 include an offset term, Z , but this
152 can be omitted with negligible difference in calibrated DO (Bittig et al. 2018b). The use of two or more
153 calibration points to derive $G(t)$, rather than the application of a single gain-correction, is supported
154 by the average in-situ drift of 2% observed in the 60 GOHSNAP optodes over the ~2-year deployment
155 period. This suggests that moored optode-DO will incur an error on the order of 1 % (~3 uM /kg)
156 per year of in-situ deployment, making the derivation of a time-dependent gain-correction factor from
157 at least two calibration points in time necessary. As a note, some optode manuals recommend that
158 optode calibrations are performed onboard the ship using a 100% oxygen saturation calibration point.
159 This typically involves having the optode log in free air for several hours before or after deployment, or
160 for several days while immersed in a water tank aerated using an aquarium bubbler. In addition to
161 the fact that only in-situ DO measurements can capture bias in optode-DO time series incurred from
162 reversible drift, which reverses once the optode is recovered to the ship, calibration with CTD-DO profiles
163 is advantageous over saturation-calibrations for moored deployments because it enables calibration to a
164 range of temperatures, DO, and pressures, rather than a single point, as with saturation-calibrations. It
165 also avoids issues of sensitivity of in-air optode behavior to humidity and temperature stability, and of
166 inadvertent over-saturation in aerated water baths.

167 There are two types of CTD-DO profiles that must be collected in order to derive $G(t_1)$ and $G(t_2)$:
168 the first is the aforementioned "cal-dip," in which the optodes are affixed to the CTD frame and dual
169 optode-DO and CTD-DO profiles are obtained, not necessarily at the mooring site. The second is a
170 "cal-cast," in which a CTD-DO cast is performed as close as possible to the mooring site where the
171 optodes are deployed and actively sampling in-situ. CTD-DO from cal-casts are matched to optode-DO
172 using temperature and salinity (collected by a sensor co-located with the optode on the mooring), since
173 cal-cast data at the pressure level of the optode might sample a different water mass due to heaving or
174 spatial gradients. Details on protocols for the collection of both cal-dips and cal-casts are described in
175 Sections 4.1 and 4.2, which include collection of Niskin bottle samples at strategic depths along each
176 profile. This is because all collected CTD-DO profiles must be calibrated using Winklers (Sections 4.3
177 and Section 4.4; Appendix B).

178 The major aspects of optode deployment, processing, and calibration, summarized in Figure 1, are:
179 a) the deployment and recovery of the moored optodes, along with the collection of necessary CTD-DO
180 profiles (blue boxes; Sections 3 and 4.1), b) the calibration of the CTD-DO profiles using Winkler-analyzed
181 bottle samples (orange boxes; Sections 4.3 and 4.4), and c) the processing and calibration of optode
182 data, which includes conversion of raw optode outputs to DO concentrations and the calibration of the

183 resulting optode-DO time series using Winkler-calibrated CTD-DO profiles (green boxes, Section 5).

184 **3 Instrument considerations**

185 **3.1 Instrument acquisition**

186 The most widely-used optodes in the oceanographic community are those with a silicone-based membrane,
187 such as the Sea-Bird Electronics (SBE) 63, Aanderaa 3830/4330, and the slow variant of RBRcoda
188 TODO. Because of their widespread usage for nearly two decades, the behaviour and drift characteristics
189 of this type of optode are better documented and characterized in the literature (e.g., Bittig and
190 Körtzinger 2017; Bushinsky and Emerson 2013; Bushinsky et al. 2016; D'Asaro and McNeil 2013;
191 Johnson et al. 2015; Ren et al. 2023) than those with membranes made from other materials. The
192 protocols for optode calibration in this paper were developed based on the analysis of data from moored
193 Aanderaa 4330 optodes and existing literature on the performance of SBE 63 and Aanderaa 3830/4330
194 optodes. Therefore, we recommend the use of optodes with a standard silicone membrane, specifically a
195 Pts3 membrane (PreSens, Regensburg, Germany) until differences, if any, in the behavior of alternative
196 sensing foil materials become better characterized.

197 When purchasing optodes, the user should ensure that they have been multi-point factory calibrated
198 and subjected to the aforementioned pre-conditioning procedure known as "burn-in" or "pre-maturation"
199 to increase stability. Because the parameters in Equation 1 are sensing-foil-/optode-specific, multi-point
200 factory calibrations for each optode will allow for higher accuracy than the alternative of "batch" factory
201 calibrations, in which the results of the multi-point calibrations of a subset of foils are extrapolated to an
202 entire batch (Bittig et al. 2018b). Most optodes can be procured with an integrated data logger, or else
203 a compatible logger must be acquired separately. The sensor/logger system should be powered by a
204 high-quality lithium-metal/ion battery pack intended for long-duration deployments. The design of the
205 sensor-logger system should enable easy battery pack service while at sea.

206 It is important to note that each optode on the mooring line needs to be co-located in depth with
207 a CTD in order to provide the temperature, salinity, and pressure measurements necessary for calibration,
208 processing, and interpretation. Temperature and salinity are used for matching water masses between
209 the mooring and cal-casts, while pressure is used for the optimization of P_{corr} in Equation 1. Salinity
210 is also used in the calculation of S_{corr} . The optode itself measures temperature close to the sensing
211 foil, as temperature is required to calculate ϕ_0 , K_{sv} , and S_{corr} in Equation 1. Because the factory
212 coefficients for these terms were developed using the optode's temperature probe readings, and because
213 these readings are located as close as possible to the sensing foil, the optode temperature should be
214 used in these calculations. However, for water mass matching, we recommend using temperature from a
215 co-located CTD, as these measurements are typically well-calibrated and come with specifications on
216 accuracy and precision.

Term	Definition
Calibration, factory	Calibration performed by the manufacturer prior to shipment. Provides some of the coefficients used in Equations 1 (for optodes) and B1 (for electrodes) but additional, in-situ calibration by the user is required.
Calibration, in-situ	Calibration performed using calibration points derived from in-situ (i.e., in the temperature, salinity, DO, and/or pressure conditions experienced by the optode during its deployment period, as opposed to laboratory or on-deck calibration) measurements taken during or shortly before/after the deployment period.
Cal-cast	A “calibration-cast” performed in the immediate vicinity of the mooring in order to obtain CTD-DO profiles co-located with the actively deployed optodes.
Cal-dip	A “calibration-dip” cast performed in which the optodes are strapped to the shipboard CTD profiler frame in order to obtain dual CTD-DO and optode-DO profiles.
CTD	A conductivity-temperature-depth (CTD) sensor.
CTD-DO	CTD-dissolved oxygen depth-profiles collected from the shipboard CTD profiling asset.
Electrode	An electro-chemical DO sensor (as opposed to an optical DO sensor) employed on shipboard profiling assets to provide CTD-DO profiles. Calibrated using Winklers.
Irreversible drift	The irreversible drift experienced by optodes across their storage and deployment periods. Occurs most rapidly within the first few years following factory calibration.
Optode	An optical DO sensor based the principles of luminescence quenching.
Optode-DO	Dissolved oxygen collected from an optode.
Processing	Calculation of DO concentrations from the raw instrument output, e.g. voltage or phase shift. See Equation 1.
Reversible drift	The exponential drift experienced in the first days to months of deployment by some optodes moored at depths greater than 1000m. Reverses once the optode is recovered to the surface.
Winklers	Discrete oxygen measurements made by Winkler-titrating bottled seawater samples.

Table 1: Glossary

217 **3.2 Optode handling and preparation**

218 When handling the optode, care should be taken to avoid touching the optode sensing foil or exposing it
219 for extended periods to sunlight. A pre-soak for at least 24-48 hours prior to any data collection - cal-dip
220 or deployment- is required for all optodes. This is due to the so-called "wetting" effect: the optode
221 foil sometimes dries out during transport or improper storage, which can affect oxygen measurements
222 by 1-2% until the foil fully re-hydrates over the course of hours or days (Aanderaa Data Instruments
223 2018). This makes a pre-soak especially crucial for the quality of optode data collected on cal-dips,
224 which take place over the course of only several hours. This soak should be performed in a covered
225 bucket to prevent sunlight from degrading the optode foil (Palevsky et al. 2023).

226 Several measures can be taken in preparation for deployment to ensure the quality and ease of
227 post-processing of the collected oxygen data, such as clock synchronization and synchronization of
228 the sample intervals for co-located instruments. Where applicable, the salinity setting in the optode
229 deployment software should always be set to 0; otherwise, the software will apply a salinity correction to
230 the oxygen measurements using a default salinity of 35. Best practice entails performing this salinity
231 correction (S_{corr} in Equation 1) in post-processing using measured salinity from the CTD (Section 5.1).
232 Lastly, optode sampling should be scheduled to begin before or during the mooring's descent through the
233 water column, or else or as soon as possible following deployment. This is to ensure that reversible drift
234 is fully captured, as it can take effect within hours of deployment. However, if the optode is connected
235 to a pump, the user must take care that it does not run while still on deck, in air.

236 **4 CTD-DO collection, processing, and calibration**

237 CTD-DO profiles from shipboard cal-dips and cal-casts are central to the processing and calibration of
238 optode-DO and therefore to the accuracy of the final, calibrated optode-DO. These CTD-DO profiles,
239 which are collected from electrodes rather than optodes, must themselves be calibrated with Winklers
240 collected at strategically chosen depths along the oxygen profile. The primary focus of this section is to
241 describe how, where, and when cal-dips and cal-casts should be performed and how to determine at
242 what depths Niskin bottles samples should be collected. A brief overview is provided on bottle sample
243 collection and Winkler analysis; however, because the quality of Winklers is highly dependent on the
244 skill of those collecting and analyzing the bottle samples, it is assumed that the science team either
245 includes an experienced Winkler analyst or is working with a trained technician who will participate in
246 the mooring deployment and recovery cruises. Handling of bottle samples and Winkler analysis by those
247 without prior experience will risk the quality of CTD-DO, and therefore the calibration of optode-DO.
248 Science teams that regularly conduct shipboard Winkler analyses will typically have a workflow in place
249 for the use of the Winklers to calibrate CTD-DO. Section 4.4 provides an overview of our recommended
250 practices for this calibration, with detailed protocols found in Appendix A.

251 **4.1 Cal-dips and Cal-casts**

252 Every optode must undergo a cal-dip on the mooring deployment cruise, prior to their deployment. To set
253 up a cal-dip, optodes should be securely attached to the frame of the shipboard CTD profiler with their
254 sensing foils facing downward and away from the frame; this avoids particles settling on the foils. One
255 method for attaching optodes to the frame is to secure ratchet straps between the top and bottom rungs
256 of the frame, and affixing the optodes to the straps using hose clamps and zip ties, as in Figure 5. The
257 cal-dip does not need to be close to the mooring site and can be performed anywhere in the region with
258 a similar water mass structure, provided that it is done: a) within days of the mooring deployment and b)
259 to depths greater than 1000 m and to at least the same depth as the planned mooring deployment. The
260 first requirement aims to minimize the amount of irreversible drift that can occur between the cal-dip
261 and optode deployment and, therefore, preserve the accuracy of $G(t_1)$ derived from the cal-dip. We
262 found that $G(t_1)$ derived from cal-dips performed within 10 days prior to mooring deployment generally
263 agreed with $G(t_1)$ derived from deployment-cruise cal-casts to within 1%. The second requirement
264 ensures adequate characterization of P_{corr} in Equation 1. It also allows for greater confidence in $G(t_1)$
265 derived from the ratio of the CTD-DO and optode-DO profiles by capturing more stable, deep water
266 masses; a portion of the profile in the upper ocean is typically excluded from this calculation due to high
267 variability and the differing response times of the CTD electrode and the optode.

268 Cal-casts should be performed at each mooring site on the deployment cruise, and again on
269 the recovery cruise. As cal-casts are meant to provide concurrent CTD-DO with the moored optode
270 measurements, they are ideally performed *after* the mooring has been deployed on the deployment cruise,
271 and *before* the mooring has been recovered on the recovery cruise. In practice, the order of operations
272 on a complex mooring cruise can depend on many factors; it is imperative that cal-casts are collected
273 at each mooring site even if they do not adhere to these strict criteria on timing. The depth of the
274 cal-cast should exceed the deepest optode by at least 100 m to ensure matchups of sampled CTD-DO
275 and optode DO in temperature-salinity space in the event of heave or lateral variability between the
276 mooring and cal-cast site.

277 **4.2 Niskin sampling**

278 The CTD-DO profiles collected on cal-dips and cal-casts are calibrated using Winkler samples from
279 Niskin bottles. To ensure optimal CTD-DO calibration for these critical casts, we recommend that bottle
280 samples be collected for every cal-dip and cal-cast. Here, we provide recommendations to help determine
281 optimal points for Niskin sampling.

282 The downcast profile should be examined during collection to identify depths at which to sample
283 oxygen during the up-cast, with the goal of prioritizing samples from:

- 284 1. Stable water masses, as this increases confidence that the CTD and the Niskin bottle will sample
285 the same water masses. Ideally, all sampling depths will be within a well-mixed layer in which
286 CTD-DO readings are constant for at least several tens of meters.
- 287 2. Extrema, as this provides the broadest possible range of oxygen concentrations to use for calibration.

288 We note that while the oxygen maximum is a useful point for calibration, it is often near the
289 surface, which is not typically a stable water mass. If this is the case, prioritize sampling of a
290 deeper local maxima and only sample the near-surface if the capacity for sample analysis allows.

291 3. A range of depths, as this allows for optimal CTD-DO calibration (See Appendix B). We recommend
292 sampling the deepest stable water mass on each cal-dip and cal-cast if resources allow, as this will
293 improve the calibration of the E term in Equation 7 used to convert the raw electrode output to
294 DO.

295 The CTD cast operator should stop fully at each Niskin sampling depth to ensure that the DO
296 sensors have stabilized before firing the Niskin. Optodes have a longer response time than CTD-DO
297 sensors; we have found that a stop time of 5 minutes allows ample time for both electrode and optode
298 stabilization. Ensuring the optode stabilizes during these stops allows for Winklers to be used for its
299 calibration in the rare case that the CTD-DO profile is deemed unfit. An example CTD-DO downcast
300 profile is shown with suitable bottle-sampling depths highlighted in Figure 5b).

301 4.3 Considerations for Winkler analysis

302 Once the cal-dip or cal-cast is complete and the profiler has been secured on the deck, Niskin bottles should
303 be immediately prepared for sampling. The cruise-dedicated Winkler specialist performing the analysis
304 will already be familiar with reagent preparation, bottle sample collection, titration instrumentation and
305 software, and the fundamentals of the chemical reactions, all of which have been thoroughly covered
306 in the GO-SHIP Repeat Hydrography Manual (Langdon 2010). In brief, the key aspects for ensuring
307 high-quality Winkler measurements are as follows: Winkler measurements should produce replicates that
308 agree to within 0.1%; anywhere between 0.1- 0.2% should be flagged as suspect but may still be used for
309 calibration, and those over 0.2% error should be discarded, as greater disagreement generally indicates
310 sample contamination during collection and/or analysis. The median of replicate data should be reported,
311 consistent with Best Practice Data Standards for Discrete Chemical Oceanographic Observations (Jiang
312 et al. 2022). For the highest accuracy, the concentration of the titrant used in the Winkler determination
313 needs to be calculated using a reference standard. A high-quality standard, such as the potassium iodate
314 standard produced by Ocean Scientific International Ltd (OSIL), should be measured, at minimum, once
315 at the beginning of the cruise and a second time at the end of a cruise. At the beginning of each titration
316 session, an internal standard that has been referenced to the OSIL standard could be used.

317 Replicate bottle samples should be collected from each Niskin. Ideally, time and resources would
318 allow for duplicate Winkler measurements on each cast of the cruise. If possible, we recommend
319 prioritizing duplicate Winkler titrations over sampling at more than the 4-5 depths needed to capture
320 the full range of stable water masses on each cast. This allows for verification of the accuracy of the
321 Winkler measurements and calibrated CTD-DO data.

322 Given the time-intensive nature of completing Winkler titrations onboard the ship, collection and
323 preservation of discrete water samples for Winkler analysis is frequently delegated to multiple members
324 of the science party, possibly including those without prior experience. If this is the case, we recommend

325 planning opportunities for training and practice prior to the collection of critical samples. Furthermore,
326 since novice samplers may introduce air contamination (bubbles) more often than experienced samplers,
327 it will be especially critical to prioritize the collection of replicate samples from each Niskin.

328 Lastly, if there is no option for a trained Winkler specialist to accompany the mooring deployment
329 or recovery cruise, collection and preservation of oxygen samples for subsequent laboratory analysis on
330 land is necessary. Best practices for the storage of bottle samples are described in Zhang et al. 2002. As
331 this method deviates from the well-established best practice of performing the Winkler analysis onboard
332 the ship, all samples to be stored for delayed analysis should be collected in duplicate, or even triplicate,
333 as an additional quality control measure, and we recommend consulting with an experienced Winkler
334 analyst prior to the cruise. We also caution that issues in stored bottle samples cannot be discovered
335 until the post-cruise Winkler analysis, when no further samples can be collected, potentially jeopardizing
336 the calibration of CTD-DO and, therefore, of optode-DO.

337 **4.4 Calibration of CTD-DO with Winklers**

338 Winklers collected on cal-casts, cal-dips, and any additional CTD-DO casts on the cruise will be used to
339 calibrate the CTD-DO electrode. Here, we provide an overview of the basics of electrode calibration
340 using Winklers, with details of sensor behavior relevant to calibration in Appendix ???. As a note, the
341 protocols given here apply to SBE 43 electrodes, the sensor found on most shipboard CTD packages.

342 Different than optodes, oxygen electrodes measure a voltage proportional to the flux of oxygen
343 molecules across a polarographic membrane. Oxygen-dependent voltages are converted to oxygen
344 concentrations using a version of the oxygen calibration equation originally presented in Owens and
345 Millard 1985 and sensor-specific factory calibration coefficients. However, to produce the best possible
346 oxygen measurements, factory-provided electrode calibration coefficients must be optimized with Winkler
347 samples to 1) reflect changes in membrane permeability that have occurred since factory calibration as a
348 result of electro-chemical drift and fouling (e.g., oil, jellyfish), and 2) optimize coefficients that were not
349 factory calibrated under pressure.

350 Historically, this in- situ oxygen calibration was done for each CTD-DO profile on a cruise by
351 performing a non-linear least squares fit of the Winkler data to a calibration equation typically containing
352 5 to 8 calibration coefficients Uchida et al. 2010 and references therein). However, on mooring cruises,
353 the number of Winklers required to robustly constrain calibration equations with up to 5 to 8 coefficients
354 for each profile is often not feasible given the large scope of tasks required on the cruise.

355 In cases when the number of collected Winklers cannot constrain the number of calibration
356 coefficients in established oxygen calibration protocols given in ibid., we offer a detailed workflow
357 for calibrating CTD-DO sensors in Appendix B that includes a worked example with provided code
358 [<https://github.com/fogaren/CTD-DO-Calibration-Example>]. Briefly, we recommend using the Seabird
359 oxygen calibration equation (Equation B1) that incorporates temperature corrections from an updated
360 sensor design and includes physically motivated pressure and temperature corrections (Atkinson et al.
361 1996; Edwards et al. 2010). Using the recommended workflow and Seabird calibration equation, the
362 number of calibration coefficients that require optimization using Winkler samples is reduced to 2, which

363 reduces the number of Winklers needed to robustly constrain the coefficients.

364 5 Optode-DO processing and calibration

365 5.1 Conversion of optode phase reading to DO concentration

366 As outlined in Section 2, the phase shift registered by the optode in units of degrees or volts is converted
367 to DO concentration using the modified Stern-Volmer Equation, Equation 1 (Uchida et al. 2008). The
368 exact form of Equation 1 differs slightly across manufacturers depending on the factory-determined
369 coefficients provided. The user should, therefore, consult the instrument manual for the appropriate
370 calculation of the terms K_{sv} , ϕ_0 , and S_{corr} . S_{corr} should be calculated with in-situ salinity measurements
371 made by the co-located CTD rather than a default constant salinity value. P_{corr} should be calculated as

$$P_{corr} = 1 + \frac{p_{fac} p}{1000}, \quad (3)$$

372 where p_{fac} is a "pressure-compensation factor" that defines the magnitude of the pressure effect
373 per 1000 dbar and p is pressure in dbars. In the absence of a means of determining the optimal p_{fac} for
374 a given optode (e.g., via a cal-dip cast), P_{corr} is calculated using a manufacturer-recommended p_{fac} ,
375 typically 3.2 or 4 % per 1000 m (Bittig et al. 2015; Tengberg et al. 2006; Uchida et al. 2008) . However,
376 variation in the reported p_{fac} values for individual optodes suggests that the use of a constant p_{fac} value
377 could result in an error on the order of 1% per 1000 m for any given optode. Indeed, our analysis of the
378 60 GOHSNAP pairs of cal-dip optode-DO and Winkler-calibrated CTD-DO profiles show a range of p_{fac}
379 values from 2.5% to upwards of 4%. To address this, Bittig et al. 2018b suggested a two-step pressure
380 correction that empirically models variation in the pressure effect across optodes using temperature and
381 pressure measurements. It was developed based on BGC-ARGO data as deep as 2000 m and has a
382 reported uncertainty of 0.3 % per 1000 dbar Bittig et al. 2015. However, the most accurate method of
383 accounting for the pressure effect is to directly determine p_{fac} individually for each sensor using a cal-dip.

384 The optimal p_{fac} for an individual optode is determined through a comparison of the cal-dip
385 optode-DO, calculated from Equation 1 omitting the P_{corr} term, and Winkler-calibrated CTD-DO
386 profiles. Equation 1 is calculated iteratively with values of p_{fac} in P_{corr} from 0.01 to 0.05 (i.e., 1-5%
387 per 1000 m). The value of p_{fac} that minimizes the root-mean-square error (RMSE) between the
388 pressure-corrected optode-DO profile and the corresponding CTD-DO profile is the optimal p_{fac} for
389 that optode (e.g., Figure 6). In our calculations, data above 500 m were excluded due to potential
390 hysteresis and noise between the optode-DO and CTD-DO that can occur in the strong oxygen gradients
391 encountered in near-surface waters. Users may need to adapt this approach to remove other sections of
392 their profiles collected in strong oxygen gradients. Once the optimal p_{fac} is determined for an individual
393 optode, the full Equation 1 including P_{corr} , can then be calculated for all optode data, that is, both the
394 cal-dip profile and the time series collected for the duration of the moored deployment. Hereafter, all
395 references to optode-DO assume calculation using optode-specific values of p_{fac} .

396 Optode-DO calculated from Equation 1 is in units of $\mu\text{mol L}^{-1}$ and can be converted to $\mu\text{mol kg}^{-1}$

Depth [m]	τ [days]	Magnitude [%]	Magnitude [$\mu\text{mol kg}^{-1}$]
1400	4.8	1.8	5.1
1993	2.4	1.7	4.5
2000	21.6	2.9	7.7
2557	2.2	2.1	6.2
2878	2.2	1.3	3.4
3124	37.6 (4.9, 32.7)	2.9 (1.4, 1.5)	7.3 (4.0, 3.3)
3334	43.7 (4.4, 39.3)	3.8 (1.2, 2.6)	10.8 (3.5, 7.3)

Table 2: Characteristics of best-fit exponential for optode-DO determined to exhibit reversible drift. For exponential functions of the form of Equation 4, the time constant is calculated as $\tau = 1/b$ and the magnitude as $(a/(a+c))$. For optodes exhibiting reversible drift on multiple time scales (i.e., "slow" on the order of weeks and "fast" on the order of days), the sum is given with the individual "fast" and "slow" components given in parenthesis.

³⁹⁷ by multiplication with $1000/\sigma_\theta$, where σ_θ is the potential density of water referenced to the sea surface
³⁹⁸ (Bittig et al. 2018a). Units of $\mu\text{mol kg}^{-1}$ are preferred when oxygen is used as a passive tracer, because
³⁹⁹ oxygen concentration per unit mass is independent of changes in temperature and pressure.

400 5.2 Detection and removal of reversible drift

⁴⁰¹ The working definition of reversible drift is an exponential decay at the start of an optode-DO time series
⁴⁰² that occurs in the absence of a similar decay in the co-located temperature time series. We recommend
⁴⁰³ that the reversible drift be removed only when there is no corresponding change in temperature in order
⁴⁰⁴ to avoid inadvertent removal of real DO changes associated with changes in temperature-dependent
⁴⁰⁵ solubility or movement of different water masses past the mooring site. The user may wish to also
⁴⁰⁶ consider the salinity time series in regions where salinity provides additional information on dynamical
⁴⁰⁷ processes. The exponential decrease in DO associated with reversible drift can appear on multiple time
⁴⁰⁸ scales, loosely categorized as "fast drift" (time scales on the order of days) and "slow drift" (time scales
⁴⁰⁹ on the order of weeks to months) (Berx et al. 2019). A single optode can exhibit reversible drift on both
⁴¹⁰ time scales. The observed reversible drift is most pronounced in the optodes deployed below 1000 m:
⁴¹¹ above 1000 m, the reversible drift – if it exists – is indistinguishable from the sensor noise and natural
⁴¹² variability.

⁴¹³ One way to separate natural variability in DO from decay related to reversible drift is as in ibid.,
⁴¹⁴ who removed temperature-driven variability from each DO time series prior to examining it for drift. This
⁴¹⁵ was done by fitting a relationship between temperature anomalies and DO anomalies for each optode-DO
⁴¹⁶ time series. This can be helpful in cases where the temperature-DO relationship has low variability;
⁴¹⁷ however, in the relatively variable GOHSNAP optode-DO time series, the fitted relationships had high
⁴¹⁸ RMS error and were not suitable for this approach. Instead, we suggest the following steps to identify
⁴¹⁹ and remove reversible drift, which are based on the characteristics of reversible drift observed here and
⁴²⁰ reported by ibid. These should be applied to every optode-DO time series deployed at depths greater
⁴²¹ than 1000 m.

422 1. Evaluate optode-DO time series for fast reversible drift

423 (a) Fit an exponential of the form

$$y = ae^{-bt} + c \quad (4)$$

424 to the first 15 days of the optode-DO time series, where a , b , and c are determined via
425 least-squares and t is in units of elapsed time (e.g., days). Calculate the exponential time
426 constant, τ as $1/b$, taking care to account for sampling interval in interpreting the resulting
427 units of time.

428 (b) Repeat Step 1a for the first 15 days of temperature from the CTD co-located with the optode.

429 (c) The optode-DO time series likely exhibits fast drift if the following are true:

- 430 i. A fit of the form of Equation 4 is found for the first 15 days of the optode-DO time
431 series by the least-squares curve fitting function
- 432 ii. Either no optimal exponential fit is found for the first 15 days of temperature, or if
433 an optimal fit is found, τ of the temperature fit is not within several days of τ of the
434 optode-DO fit.
- 435 iii. The magnitude (a) of the exponential function fit to the optode-DO is greater than
436 twice the standard deviation of the first 15 days of optode-DO. This criterion helps to
437 distinguish drift from natural variability.

438 2. If the optode-DO time series is determined to exhibit fast drift, remove the drift by subtracting
439 ae^{-bt} from the first 15 days (e.g., Figure 8).

440 3. Evaluate optode-DO time series for slow reversible drift. If fast drift was identified in the previous
441 step, use the fast-drift-corrected time series for the following steps:

442 (a) Detrend the full optode-DO time series. This isolates potential reversible drift from any
443 quasi-linear trends present due to long-term natural variability or irreversible drift.

444 (b) Fit Equation 4 to days 6 through 300 of the optode-DO time series, or the full optode-DO
445 time series, whichever is shorter. Excluding the first 5 days avoids any influence from fast
446 drift on the fit for slow drift. Limiting the time period over which Equation 4 is fit to 300
447 days or less helps to constrain the fit to the time scales at which slow reversible drift has been
448 observed, typically with decay time constants on the order of weeks (Table 2), and avoid
449 fitting to longer-term variability unrelated to reversible drift.

450 (c) Repeat Steps 3a and 3b for the co-located temperature time series

451 (d) The optode-DO time series likely exhibits slow reversible drift if the following are true:

- 452 i. An optimal fit of the form of Equation 4 is found for days 6 through 300 of the optode-DO
453 time series by the least-squares curve fitting function
- 454 ii. Either no exponential fit is found for the first 300 days of temperature, or if a fit is found,
455 τ of the temperature fit is not within about 20 days of τ of the optode-DO fit.

456 iii. The magnitude (a) of the exponential function fit to the optode-DO is greater than
457 twice the standard deviation calculated across the full time series. On this time scale,
458 seasonal variability can cause large variations in dissolved oxygen that may be mistaken
459 for reversible drift if sampling begins during a seasonal decline in oxygen.

460 (e) If the optode-DO time series is determined to exhibit slow drift, remove the drift by subtracting
461 ae^{-bt} from the time period over which Equation 4 was fit, days 6 through 300 .

462 Of the 24 optodes on the OSNAP array that were deployed at depths greater than 1000 m, we
463 diagnosed reversible drift in 7 (Figure 7) using these criteria. Of these 7 optodes, 6 exhibited fast decay
464 with exponential time constants (τ) ranging from 2 - 5 days and magnitudes from 1.5 - 2.1% (Table 2)
465 and 3 exhibited slow decay, with magnitudes of 1.2 -2.9% and time constants of 21-40 days. Two of
466 these 7 exhibited both slow and fast decay. Figure 9a and b show an example optode-DO time series with
467 a clear exponential decay that is absent in the paired temperature time series, suggesting (slow) reversible
468 drift based on the criteria above. Figure 9c and d show an example in which both the optode-DO and
469 temperature time series exhibit exponential behavior with similar time constants, suggesting the decline
470 in dissolved oxygen is a real physical occurrence rather than an artifact of reversible drift. Figure 9e is
471 an example of where a fit to Equation 4 was found over the first 300 days of the optode-DO but not
472 in the temperature time series (latter not shown). However, we decided that this exponential decline
473 should not be attributed to reversible drift because (a) the fit doesn't appear representative of the visual
474 trace data over which it was calculated and (b) the magnitude of the fit does not exceed the standard
475 deviation calculated across the full time series (criteria 1(c)iii and 3(d)iii). Furthermore, the initial decay
476 in question appears to be the declining portion of a regular seasonal cycle in which DO increases in
477 the spring and summer months and declines through fall and winter, i.e. context suggests that the
478 initial decay could be a real decrease rather than a result of drift. This case highlights the necessary role
479 of subjective analysis when applying the suggested criteria. While the use of least-squares fitting and
480 calculation of standard deviations provide some measure of objectivity, at present, the determination of
481 whether an optode-DO time series exhibits reversible drift ultimately rests on the analyst's judgement of
482 the how reasonably the exponential fit represents the time series as well consideration of the criteria in
483 the context of local hydrography and variability at the mooring site. As more in situ data from moored
484 oxygen optodes are obtained and analysed, we anticipate that lessons from those results will enable
485 future refinements to these steps that will reduce the need for subjective analysis.

486 5.3 Removal of irreversible drift

487 At this step in the handling of optode-DO, raw optode phase readings have been converted to DO
488 concentrations, the optimal p_{fac} for each optode has been determined and applied to both the optode-DO
489 cal-dip profile and deployment time series, and all optodes deployed at depths ≥ 1000 m have been
490 examined, and if applicable, corrected, for reversible drift. The final step is to correct for irreversible
491 drift, i.e., to calibrate each optode-DO time series against the deployment and recovery CTD-DO profiles
492 (Figure 1). As outlined in Section 2, this is done by multiplication of the optode-DO time series with

493 a time-dependent gain correction, $G(t)$, a linear fit between two calibration points, $G(t_1)$ and $G(t_2)$
 494 (Equation 2). These calibration points are calculated at the beginning and end of the optode-DO time
 495 series as a ratio of optode-DO to Winkler-calibrated CTD-DO:

$$G(t_i) = \text{mean}(CTD\text{-}DO/Optode\text{-}DO) \quad (5)$$

496 For the initial calibration point, $G(t_1)$, this ratio is most robustly calculated from full, co-located
 497 water column profiles of optode-DO and CTD-DO; that is, cal-dip profiles. This is additionally advan-
 498 tageous because it leaves the deployment cruise cal-cast profile as a means of independent validation.
 499 However, in cases where reversible drift causes additional bias beyond the irreversible drift captured
 500 by the cal-dip, $G(t_1)$ should be calculated from the deployment cruise cal-cast CTD-DO matched in
 501 temperature and salinity to the moored optode-DO instead. We recommend that until reversible drift is
 502 better constrained, the final calibration point, $G(t_2)$, is calculated using cal-cast CTD-DO, regardless of
 503 whether reversible drift was identified in the optode-DO time series; this ensures that any undetected
 504 reversible drift that has accumulated over the deployment period is captured.

505 When calculating $G(t_1)$ from Equation 5 using cal-dip profiles, the profiles should exclude the
 506 highly-variable surface layer, which can cause hysteresis between the oxygen profiles. In our calculations,
 507 Equation 5 was evaluated for the profiles from 500 m to the deepest point of the profile (e.g., Figure
 508 4a). When calculating either $G(t_1)$ or $G(t_2)$ from cal-cast data, Equation 5 is evaluated using CTD-DO
 509 from the cal-cast and optode-DO from +5 days of the date of the cal-cast that have been matched
 510 in temperature-, salinity-, and pressure- space. This ensures a comparison of DO from the same
 511 water mass. A "good" match between the water masses sampled by the optode and by the CTD
 512 should result in a standard deviation in the ratio of $CTD\text{-}DO/Optode\text{-}DO$ of less than 0.01. This is
 513 because a difference of ± 0.01 in $G(t_i)$ yields differences in calibrated optode-DO on the order of $\pm 1\%$,
 514 which is within the accuracy specification reported by manufacturers for multi-point factory calibrations
 515 ([aanderaa`data`instrumentss`aanderaa`2018](#); SeaBird Electronics 2023). For the GOHSNAP dataset,
 516 a threshold of 0.005°C , a salinity threshold of 0.005, and a pressure threshold of ± 100 dbar yielded
 517 suitable standard deviations in $G(t_i)$ (Figure 4b). The user will need to adjust these thresholds according
 518 to their data in order to achieve a standard deviation of 0.01, and can additionally choose to narrow the
 519 time-window of optode-DO relative to the cal-cast date.

520 Once $G(t_1)$ and $G(t_2)$ are determined, $G(t)$ is calculated as a linear relationship between these
 521 two points.

$$G(t) = mt + b \quad (6)$$

522 where $m = \frac{G(t_2) - G(t_1)}{t_2 - t_1}$ and t is in the same units of elapsed time as in Equation 4. $G(t)$ may then be
 523 used in Equation 2 to obtain the final, calibrated optode-DO time series (Figure 4c). Code examples
 524 of the step-by-step processing and calibration of optode-DO with and without the reversible drift are
 525 available at https://github.com/unamiller/optode_processing_examples/tree/main.

526 **6 Uncertainties and validation**

527 The steps described in Section 5 are aimed at reducing uncertainties and achieving the most accurate
528 moored optode-DO time series possible. As with any data product, however, uncertainties remain in the
529 final calibrated optode-DO time series. The largest source of uncertainty is from the calibration process,
530 in which both the trend and magnitude of the calibrated optode-DO time series are essentially set by two
531 calibration points, $G(t_1)$ and $G(t_2)$. Inaccurate $G(t_1)$ or $G(t_2)$ can therefore introduce bias and artificial
532 trends in the calibrated optode-DO time series and is why proper Winkler calibration of CTD-DO, as
533 well as careful matching of water masses between cal-casts and mooring sites, are essential.

534 As $G(t_1)$ and $G(t_2)$ are calculated from the mean ratio of CTD-DO to optode-DO (Equation 5),
535 the standard deviation of the ratio reflects error in the oxygen measurements or in the matching of their
536 respective water masses. If the optode and CTD electrode are accurate and sampling precisely the same
537 water mass at the same time, their ratio should be consistent across each data point, i.e., low variance
538 about the mean. This is exemplified by cal-dips, where the typical RMS error between the two profiles
539 is less than $1 \mu\text{mol kg}^{-1}$ (e.g., Figure 6), equivalent to uncertainty of less than 0.3 % in the resulting
540 calculation of Equation 5 for our data. $G(t_1)$ or $G(t_2)$ derived from cal-casts, however, will take on
541 greater error due to spatial and temporal variability in dissolved oxygen between the mooring site and the
542 cast site, as well as any error in the accuracy of the temperature and salinity measurements used to match
543 water masses. The use of a 0.01 limit for the standard deviation of the ratio of *CTD-DO/Optode-DO*
544 (Equation 5) when matching water masses is an attempt to limit uncertainty in $G(t_1)$ or $G(t_2)$, such that
545 uncertainty in the resulting calibrated optode-DO is approximately 1% (Section 3). Because cal-casts are
546 used to calculate both $G(t_1)$ and $G(t_2)$ in optode-DO time series corrected for reversible drift, these time
547 series will have higher uncertainty related to their calibration than time series without reversible drift,
548 which use cal-dips for the calculation of $G(t_1)$. This is in addition to any uncertainty in least-squares fit
549 of the exponential function to the reversible drift trace.

550 Serendipitous CTD-DO casts taken at three of the OSNAP array mooring sites mid-way through the
551 optode deployment period allow us to assess uncertainty in the calibrated optode-DO time series using
552 data fully independent of the calibration process (Figures 10, 11, 12). These CTD-DO were matched to
553 each of the 11 optodes at the three mooring sites using the same temperature, salinity, and pressure
554 thresholds described in Section 3. Average error between the optode-DO and cal-cast CTD-DO ranged
555 from 0.26 to $8.87 \mu\text{mol kg}^{-1}$ with a median of $2.40 \mu\text{mol kg}^{-1}$ and a mean of $2.67 \mu\text{mol kg}^{-1}$. The
556 two highest average errors, 8.87 and $4.55 \mu\text{mol kg}^{-1}$ were found in the two shallowest optodes at 77
557 and 530 db (Figure 10a,b), where spatial and temporal variability in dissolved oxygen, and therefore
558 error, between the cal-cast and mooring site are likely elevated due to biological activity and patchiness
559 in convective processes.

560 Notably, despite the larger uncertainties associated with the correction of optode-DO with reversible
561 drift, the three optodes with reversible drift did not have error that was systematically higher than those
562 without. Error in these three optodes was 2.81 , 3.23 , and $1.53 \mu\text{mol kg}^{-1}$ at 1993 db, 2000 db, and
563 2557 db, respectively, compared to the average error across all 11 optodes of $2.67 \mu\text{mol kg}^{-1}$. Overall,
564 the average error of $2.67 \mu\text{mol kg}^{-1}$ is roughly 1% of calibrated optode-DO and consistent with the

estimated 1% uncertainty associated with the use of cal-casts to derive $G(t_1)$ and $G(t_2)$. This suggests that uncertainty in the calibrated optode-DO time series is broadly $\sim 1\%$ across the deployment period and that the leading source of uncertainty is from the matching of water masses between the cal-cast and mooring site, even for time series that were corrected for reversible drift.

In most cases, CTD-DO casts are not performed at mooring sites outside of the deployment and recovery cruises. DO profiles from optodes on BGC-Argo floats (BGC-Argo-DO; Thierry et al. 2021) provide an alternative means of validation for optode-DO calibrations. It should be noted, however, that BGC-Argo have their own uncertainties associated with "delayed-mode" correction protocols that are reported in the range of 1 - 3 % ($\pm \sim 3 - 9 \mu\text{mol kg}^{-1}$) (Johnson et al. 2015; Maurer et al. 2021; Mignot et al. 2019; Takeshita et al. 2013). This range is consistent with the relatively low median errors between BGC-Argo-DO and GOHSNAP optodes, which were generally near or below 1% (Table 3). BGC-Argo-DO profiles can be matched to moored optode-DO using the same time, temperature, salinity, and pressure criteria used to match cal-cast profiles to the moored optodes, though we found more relaxed criteria yielded similarly low errors. Only "delayed mode" BGC-Argo-DO profiles should be considered, as these have undergone a greater degree of quality-control and data correction than "adjusted mode" or "real-time" profiles. We found that a relatively large search radius (100 km, centered at each mooring site) for BGC-Argo-DO profiles in OSNAP study region still yielded helpful comparisons when filtered using strict temperature and salinity criteria, though some regions may require a smaller search radius. Code for accessing the BGC-ARGO repository and matching with the OSNAP moorings may be found at https://github.com/ellenrpark/bgcargo_floatmatchup.

As an example of the value of the comparison with BGC-Argo profiles, we used BGC-Argo-DO to verify a steady decline in optode-DO observed across the deployment period at mooring sites "M2" and "M3" (Figure 11, 12). A potential concern in interpreting this trend was that, rather than reflecting a real physical process, our results might instead have been indicative of a systematic error in the Winkler calibrations of CTD-DO at these two sites. However, both BGC-Argo profiles and the mid-deployment cal-casts validate the calibrated optode-DO, suggesting that the decline is a real phenomenon. In particular, BGC-Argo-DO available across the full deployment period at M3 1012 db independently shows the same decline (Figure 12a).

As a final point, cross-validation of optode-DO against CTD-DO, BGC-Argo-DO, and other platforms, such as gliders, will promote the cohesion and interoperability of dissolved oxygen datasets within the oceanographic community.

7 FAIR data archiving

To maximize the impact and future use of moored dissolved oxygen observations we recommend applying Findability, Accessibility, Interoperability and Reuse (FAIR) data principles when organizing data products (Wilkinson et al. 2016). The international Climate and Ocean Variability, Predictability and Change (CLIVAR) program outlines a data policy that includes principles of free and unrestricted exchange, metadata, quality control, data preservation, reusability and easy access. Ideally, this should include

Matching criteria	Overall	Air	CTD-NCEP	CTD-WOA	WOA
1	23 0.79 (0.49)	10 1.19 (0.41)	8 1.92 (0.81)	2 -2.67 (0.90)	3 -0.91 (0.31)
2	16 -0.40 (0.5)	5 2.64 (1.12)	7 0.91 (0.50)	4 -1.01 (0.35)	
3	107 -1.48 (1.05)	20 1.89 (1.23)	70 -1.68 (0.93)	12 -1.05 (0.47)	5 -5.35 (1.87)

Table 3: Error between BGC-ARGO-DO and GOHSNAP moored optode-DO. Matching criteria used to match the Argo profiles and optodes are: Row 1) $/pm$ 0.005 $^{\circ}$ C potential temperature, $/pm$ 0.005 practical salinity, and $/pm$ 100 db for pressure, Row 2) $/pm$ 0.01 $^{\circ}$ C, $/pm$ 0.01, and $/pm$ 10 db, respectively, and Row 3) $/pm$ 0.01 kg m⁻³, and $/pm$, respectively. All matches were restricted to \pm 5 days of the Argo profile date and within 100 km of the mooring site. The categories of delayed-mode Argo data corrections are in-air ("Air"), combined CTD-DO profiles and National Centers for Environmental Protection (NCEP) climatology (CTD-NCEP), combined CTD-DO profiles and World Ocean Atlas climatology (CTD-WOA), and WOA climatology. For each category, the number of matched profiles is given followed by the median error in $\mu\text{mol kg}^{-1}$ (calculated as optode-DO – BGC-ARGO-DO), with relative error in % (calculated as optode-DO – BGC-ARGO-DO)/optode-DO) in parenthesis.

602 the whole chain of data required to reproduce final products, including shipboard discrete sample (e.g.
 603 Winkler) and CTD data, optode as well as CTD measurements from cal-dips, raw moored optode data
 604 and final calibrated versions.

605 For discrete bottle data, current best practices (Jiang et al. 2022) outline standards for column
 606 headers, units, quality flags, etc. in accordance with practices of the Carbon Hydrographic Data Office
 607 (CCHDO) at Scripps Institution of Oceanography.

608 Moored data is best reported using a format that includes data and metadata, such as NetCDF.
 609 The data model should follow existing exemplars such as the Climate and Forecast (CF) conventions
 610 (Hassell et al. 2017) and the Argo data manual (Thierry et al. 2022). Quality-controlled moored
 611 oxygen data is best presented alongside an aligned time-series of temperature, pressure and salin-
 612 ity, which allows for calculations of related derived parameters such as the equilibrium saturation
 613 concentration and apparent oxygen utilization (AOU). We also recommend including the following
 614 data attributes: optode serial number, manufacturer and make, mooring ID, nominal depth, median
 615 pressure, latitude, longitude, reversible pressure correction flag (true/false), p_{fac} , $G(t_1)$, $G(t_2)$, and
 616 a description of the calibration methods. Example NetCDFs for optode-DO data can be found at
 617 https://github.com/unamiller/optode/_processing_examples/tree/main/FAIR-format NetCDF examples.

618 Finally, we note that best practices for moored biogeochemical data is actively evolving and the
 619 user should consult latest publications and community consensus to inform decisions on data model and
 620 format.

621 8 Summary

622 In this paper, we have described protocols for moored optode deployment, data processing, and
 623 data calibration, with recommendations intended to achieve the collection of high-quality optode-DO
 624 measurements. The major points are reiterated here, and the reader is again pointed to the quick-start

625 guide and worked examples made available in the Appendix and on GitHub.

- 626 1. Optodes are known to drift from factory calibration, requiring calibration against CTD-DO collected
627 on the mooring deployment and recovery cruises. This drift occurs as a time-dependent “irreversible
628 drift” and a pressure-and-time-dependent “reversible drift”, which is identified in some optodes
629 deployed at depths below 1000m. Analysis of the 60 GOHSNAP optodes over two years of
630 deployment showed irreversible drift occurring at an average rate of ~1 % per year of in-situ
631 deployment, and reversible drift ranging from 0.85 to 3.3 % per 1000 m.
- 632 2. Reversible drift in optodes has not been widely characterized outside of the present study. Our
633 observations of the 60 GOHSNAP optodes and those of Berx et al. 2019 suggest that for moored
634 optodes below depths of 1000 m, reversible drift can be identified as an exponential decay in
635 dissolved oxygen occurring within the first days (“fast reversible drift”) or weeks to months (“slow
636 reversible drift”) of deployment, in the absence of a similar change in the co-located temperature
637 time series. The amplitude of the drift ranges between 3.4 and 10.8 $\mu\text{mol kg}^{-1}$ (Table 2) or 1 to
638 3 $\mu\text{mol kg}^{-1}$ per 1000 m, and in our data, occurred largely as fast drift, that is, within the first
639 several days of deployment. We provide a heuristic protocol for the identification and removal of
640 reversible drift and emphasize the role of expert judgement in assessing and correcting for this
641 drift. As more deep-moored optode deployments are collected and analysed by the community,
642 improved characterization and thus protocols for its correction will emerge.
- 643 3. The two types of CTD casts required to calibrate moored optode-DO are cal-dips, casts on which
644 optodes are strapped to the CTD profiler and dual optode-DO and CTD-DO profiles are obtained,
645 and cal-casts, CTD-DO profiles taken as close to the mooring site as possible while the optodes
646 are sampling in-situ. These CTD casts are used to derive $G(t_1)$ and $G(t_2)$, the two gain-correction
647 factors used to derive the linear calibration function $G(t)$ used in Equation 2.
- 648 4. Cal-dips also serve as a means of determining the optode-specific pressure correction factor, p_{fac} ,
649 in the P_{corr} term of Equation 1. Our analysis of 60 optodes shows values of p_{fac} to range from
650 2.5% to 4% per 1000m, suggesting that use of a default constant value of p_{fac} would result in
651 error on the order of 1% per 1000m in an individual optode-DO time series.
- 652 5. The accuracy of calibrated optode-DO depends directly on the quality of shipboard CTD-DO,
653 which itself must be calibrated using Winklers. Because Winkler titrations are highly sensitive and
654 require a skilled analyst, any science team planning to deploy moored optodes must also plan for
655 the collection and analysis of Winklers on both the deployment and recovery cruises. On-board
656 titrations by a skilled analyst yield the highest-quality Winklers.
- 657 6. The calibration of moored optode-DO can be validated through cross-platform comparisons, such
658 as with mid-deployment CTD-DO profiles (calibrated with Winklers) and/or BGC-Argo-DO, or
659 optode-equipped gliders. Comparison of BGC-Argo-DO profiles to optode-DO matched using
660 temperature, salinity, pressure, and time thresholds yielded median relative errors of ~ 1 % or less.

661 **9 Acknowledgements**

662 We thank Overturning in the Subpolar North Atlantic Program (OSNAP), and in particular, Dr. Johannes
663 Karstensen, Dr. Dave Hebert, Dr. Marc Ringuette, Dr. Susan Lozier, Dr. Fiamma Straneo, Dr. Amy
664 Bower, and Dr. Robert Pickart for supporting us in deploying optodes on the mooring array and thereby
665 enabling Gases in the Overturning and Horizontal circulation of the Subpolar North Atlantic Program
666 (GOHSNAP). We also thank the crew and scientists aboard the 2019-2020 OSNAP mooring cruises:
667 AM2001, AR45, AR46, MSM94-01, AT48-05, AR69-03, and M184. UKM and JP were supported by
668 National Science Foundation (NSF) award 1947829. HP, KF, and MY were supported by NSF award
669 1947970. DA and JK were supported by the Canada Excellence Research Chair (CERC) in Ocean Science
670 and Technology, the Canada First Research Excellence Fund (Ocean Frontier Institute grant, Module B),
671 and the CERC.Ocean group led by Prof. Douglas Wallace at Dalhousie University. EP was supported
672 by OCE-2023080 and OCE-1947567. David Nicholson was supported by OCE-1947567. BGC-Argo is
673 supported by the Global Ocean Biogeochemistry Array (GO-BGC) Project under the NSF Award 1946578
674 with operational support from NSF Award 2110258.

675 **Appendix A Quick-start Guide**

- 676 1. Pre-deployment cruise preparation
 - 677 (a) Acquire optodes (Table 1) with a silicone-based membrane (Section 3). Keep track of the
678 manufacturer-provided factory coefficients provided for each optode.
 - 679 (b) Acquire, or ensure mooring plans, for an equal number of conductivity-temperature-depth
680 (CTD) sensors, if the optodes do not come integrated with CTDs (e.g., SBE SMP-ODO
681 microcat). Salinity, temperature, and pressure measurements are all essential to optode data
682 processing and calibration (Section 5)
 - 683 (c) Create a mooring plan in which each optode is co-located on the mooring line with a CTD
 - 684 (d) Dissolved oxygen from CTD casts (CTD-DO) are central to the processing and calibration of
685 dissolved oxygen from optodes (optode-DO). Create a cruise plan in which:
 - 686 i. Cal-dips (Table 1) are performed for each optode prior to their deployment (Section 4.1).
687 An optode sampling frequency of or around every 15 seconds is recommended for the
688 cal-dip, though this will be battery-intensive, and battery replacement may be required
689 prior to mooring deployment.
 - 690 ii. Cal-casts (Table 1) are performed at each mooring site following mooring/optode
691 deployment (Section 4.1)
 - 692 iii. Niskin bottle samples are collected for Winkler analysis on all cal-dips and cal-casts of
693 the CTD-DO (Section 4.3)
 - 694 (e) Make arrangements for Winkler analysis of the Niskin bottle samples to be performed on the
695 cruise, including ensuring that an experienced Winkler analyst will be on the cruise, along

696 with all necessary Winkler equipment and materials (Section 4.3)

697 2. Deployment cruise protocols

- 698 (a) Pre-soak optodes in a covered bucket 24-48 hours prior to their cal-dip (Section 3.2)
- 699 (b) When programming the optodes for sampling, match the clock and sampling interval with
700 that of the CTD. If the optode software provides an input for default salinity, this value should
701 be set to 0 (section 3.2)
- 702 (c) Cal-dip the optodes. Collect Niskin bottle samples for shipboard Winkler analysis at depths
703 that optimize CTD-DO calibration (Section 4.3). Keep careful records of which optode serial
704 numbers match with which CTD cast numbers.
- 705 (d) Pre-soak optodes again 24-48 hours prior to their deployment on the mooring
- 706 (e) Deploy the optodes on the mooring
- 707 (f) Perform a cal-cast as close as possible to the mooring site. Collect Niskin bottle samples for
708 shipboard Winkler analysis.

709 3. Ensure calibration of CTD-DO collected on the deployment cruise using Winklers

710 4. Recovery cruise protocols

- 711 (a) Perform a cal-cast as close as possible to the mooring site. Collect Niskin bottle samples for
712 shipboard Winkler analysis.
- 713 (b) Recover the mooring/optodes. Make note of any biofouling visible on the optodes
- 714 (c) If turning around the optodes and moorings (i.e, redeploying), repeat the Deployment cruise
715 protocols. If recovering without redeploying, perform steps 4a and 2f, prior to the mooring
716 recovery.

717 5. Ensure calibration of CTD-DO collected on the recovery cruise using Winklers

718 6. Post-deployment optode data processing

- 719 (a) Take stock of all necessary data sets:
 - 720 i. Moored optode-DO time series
 - 721 ii. Moored CTD time series
 - 722 iii. Cal-dip optode-DO profiles
 - 723 iv. Cal-dip CTD and Winkler-calibrated CTD-DO profiles
 - 724 v. Cal-cast CTD and Winkler-calibrated CTD-DO profiles
- 725 (b) Organize key metadata for each optode:
 - 726 i. Optode serial number
 - 727 ii. Optode factory calibration coefficients

- 728 iii. ID/file name for co-located moored CTD sensor
 729 iv. Mooring site ID and lat/lon
 730 v. Depth on mooring line
 731 vi. Date and cast ID for deployment cruise cal-dip
 732 vii. Date and cast ID for deployment cruise cal-cast
 733 viii. Date and cast ID for recovery cruise cal-cast
 734 ix. Any notes made during the cruises, e.g., visible biofouling

- 735 (c) Convert raw optode phase data from the cal-dip profiles to dissolved oxygen concentration
 736 using Equation 1 (reprinted below) in Section 2, omitting the pressure correction term, P_{corr}
 737 (Section 5.1)

$$[O_2] = \frac{(\phi_0/\phi - 1)}{K_{sv}} S_{corr}$$

- 738 (d) Calculate the optimal P_{corr} (Equation 6d) for each optode by finding the value of p_{fac} that
 739 minimizes the root-mean-square (RMS) error between its cal-dip optode-DO profile and
 740 respective cal-dip CTD-Do profile (Section 5.1)

$$P_{corr} = 1 + \frac{p_{fac} p}{1000}$$

- 741 (e) (Re)apply Equation 1 to the raw phase data from both the cal-dip profile and the deployment
 742 time series using P_{corr} with the optimal value of p_{fac} (Section 5.1)

$$[O_2] = \frac{(\phi_0/\phi - 1)}{K_{sv}} S_{corr} P_{corr}$$

- 743 (f) Visually examine any of the resulting optode-DO time series at depths greater than 1000m
 744 for reversible drift (Table 1), using the protocols in Section 5.2. Correct for reversible drift if
 745 found.

- 746 (g) Calibrate the optode-DO time series according to Equation 2 (Section 2)

$$[O_2]_{calibrated} = G(t)[O_2]$$

747 where $G(t)$ is calculated as linear fit between $G(t_1)$ and $G(t_2)$, two gain correction factors
 748 derived from CTD-DO collected on the deployment and recovery cruises, respectively. $G(t_1)$
 749 and $G(t_2)$ are calculated according to Equation 5:

$$G(t_i) = \text{mean}(CTD\text{-}DO/Optode\text{-}DO)$$

- 750 i. If the optode-DO time series does **not** exhibit reversible drift, $G(t_1)$ is calculated from
 751 Equation 5 as the ratio of cal-dip CTD-DO to optode-DO (Section 5.3).
 752 ii. If the optode-DO time series has, and was corrected for, reversible drift, $G(t_1)$ is
 753 calculated from Equation 5 as the ratio of cal-cast CTD-DO to optode-DO that have

been matched in temperature, salinity, and pressure space (Section 5.3). Adjust the thresholds on temperature, salinity, and pressure such that the standard deviation of *CTD-DO/Optode-DO* is 0.01 or less.

iii. For all optodes, calculate $G(t_2)$ according to Equation 5 following the same protocols as in Step 6(g)ii

(h) *Optional* Collate dissolved oxygen profiles from BGC-Argo in the vicinity of the mooring and use as a means of validation or additional context to your calibrated optode-DO time series. Note the reported uncertainties for each profile (typically included in the profile metadata), which can be as large as $\pm 9 \mu\text{mol kg}^{-1}$.

(i) *Optional* Make your moored optode-DO time series available in a manner consistent with Findability, Accessibility, Interoperability and Reuse (FAIR) data principles (Wilkinson et al. 2016) (Section 7)

Appendix B Calibration of CTD-DO using Winklers

As introduced in Section 4.4, shipboard CTD packages are often outfitted with SBE 43 dissolved oxygen sensors. This appendix has been included to provide a detailed background on SBE 43 DO sensor behavior that will be of interest to end users deciding on how to best calibrate shipboard CTD-DO profiles. The SBE-suggested calibration equation has been modified from the original form presented in Owens and Millard 1985 to incorporate an updated sensor design for temperature corrections and to include physically motivated pressure and temperature corrections (Atkinson et al. 1996; Edwards et al. 2010):

$$O_2 = S_{oc} * (V + V_{off} + \tau_{20}) * OxySol(T, S) * (1 + A * T + B(T^2 + C * T^3)) * e^{E*p/(273.15+T)}, \quad (\text{B1})$$

where V is the output voltage signal [volts], $OxySol(T, S)$ is the oxygen saturation [in desired oxygen concentration units], T is temperature [$^{\circ}\text{C}$], S is salinity [psu], and P is pressure [dbar]. S_{oc} , V_{off} , τ_{20} , A , B , C , E are calibration coefficients determined from an 18-point factory calibration and provided by the manufacturer, where S_{oc} is the calibration slope term, V_{off} is the voltage at zero oxygen signal, τ_{20} is an optional correction for the sensor response time, the temperature correction expression compensates for temperature changes on membrane permeability, and E compensates for the pressure effect on membrane permeability. V_{off} , A , B , and C remain constant over the sensor life while S_{oc} , τ_{20} and E can be optimized for the CTD-DO sensor using Winklers.

There are two mechanisms that cause S_{oc} to drift from its factory calibration. The first and largest cause of drift is fouling of the sensor membrane, which reduces permeability of the sensor membrane and sensitivity to changes in oxygen, ultimately causing the sensor to read lower than the actual oxygen concentration. This drift can be gradual as the sensor membrane accumulates material over the course of a cruise or can abruptly appear from a particular event (e.g., profiling through oil slick, jellyfish

787 intake). The second mechanism responsible for drift in S_{oc} is electrolyte consumption within the Clark
788 electrode since the SBE43 sensor is continuously polarized. This electro-chemical drift is slow and well
789 characterized (SBE Application Notes No 64 and 64-2). Regardless of the cause, drift in the calibration
790 slope term with time can be corrected by comparing sensor data to Winklers collected over the course of
791 the cruise.

792 The E calibration term, which corrects for sensor behavior based on pressure, can also be optimized
793 by comparison between sensor measurements and Winkler data. The factory-determined calibration
794 constant is determined at a pressure of 0 db. Without in-situ calibration, the application of the vendor-
795 provided E term often results in a relationship between the residuals (Winklers – CTD-DO) and pressure
796 for depths greater than 1000 m (Atkinson et al. 1996). Since E should remain stable over the life of the
797 sensor, users can do a one-time correction to tune the E term by comparing water samples from greater
798 than 1000 m to hysteresis-corrected CTD-DO sensor values (Sea-Bird Scientific University Module 28;
799 <https://www.seabird.com/training-materials-download>). If it is not possible to collect samples greater
800 than 1000 m on the cruise, users can calibrate the E term using samples collected on previous or following
801 cruises since the E term should remain constant for the sensor.

802 In addition to the calibration equation provided in Equation B1, Sea-Bird also provides two optional
803 dynamic corrections that users can apply to collected data. Starting in 2008, Sea-Bird has provided a
804 τ_{20} correction. While the τ_{20} correction aims to improve the measured signal response for large oxygen
805 gradients, it can also amplify residual noise, especially in deep, cold waters with weak oxygen gradients
806 resulting in large τ_{20} values (Edwards et al. 2010). The sensor response time correction is optional and
807 users should weigh the benefit of increased signal responsiveness against the consequence of amplified
808 residual noise in the signal. We have found the τ_{20} correction does not improve our oxygen profiles and
809 do not apply this correction.

810 Since 2010, SBE has provided an optional pressure-induced hysteresis correction. Hysteresis in
811 oxygen profiles collected with SBE 43 oxygen electrodes results from a time-dependent change in sensor
812 behavior under pressure, and can result in upcast oxygen concentrations as much as $10 \mu\text{mol kg}^{-1}$
813 lower than downcast concentrations. A dynamic correction for this time and pressure-dependent sensor
814 behavior was provided by ibid. that can be applied in post processing to correct for this behavior and
815 reduce the previously observed hysteresis between upcasts and downcasts in oxygen profiles to ~ 1
816 $\mu\text{mol kg}^{-1}$. Prior to this time-pressure hysteresis correction, calibration and scientific use of downcast
817 oxygen data was preferred over upcast data because the sensor behavior is less affected during the
818 downcast. However, application of the time-pressure hysteresis correction to an inline pumped DO sensor
819 allows users to calibrate both downcasts and upcasts using Winkler samples collected on upcasts. Note,
820 while the effects of pressure-induced hysteresis are most obvious in deep-water casts, pressure-induced
821 hysteresis occurs at all depths, and must be corrected for at all depths (ibid.). We have found the
822 default hysteresis correction to work well for correcting pressure-induced hysteresis and recommend its
823 application (SBE Application Note 64-3; <https://www.seabird.com/application-notes>).

824 Currently, SBE does not provide software for optimizing calibration equation coefficients using
825 Winkler measurements. As such, we provide the following workflow to demonstrate CTD-DO calibration

826 using Winklers using data from joint 2022 Ocean Observatories Initiative Irminger/GOHSNAP Cruise
827 (AR69-01). This workflow uses a combination of SBE Data Processing Software and processing routines
828 developed by us and others. Briefly, SBE-provided software is used to convert raw data to engineering
829 units and perform the desired data processing routines on the converted data. Detailed documentation for
830 applying these processing routines is available at <https://www.seabird.com/training-materials-download>.
831 Users may also convert raw data and apply processing routines themselves, and different CTD toolboxes
832 are available (e.g., SBE, SBE-DO, CTD-python). With dynamic oxygen corrections (e.g. pressure-induced
833 hysteresis) and oxygen sensor delay correction applied (see below), oxygen voltages are then converted
834 to concentrations using Winkler-determined calibration coefficients and corresponding measurements
835 of temperature, salinity (calibrated if possible) and pressure in the SBE provided calibration equation.
836 The code that accompanies this worked example is available at <https://github.com/fogaren/CTD-DO-Calibration-Example>. Further details and the full processed CTD-DO dataset from this cruise are
837 available from Biological and Chemical Oceanography Data Management Office (BCO-DMO) (Fogaren
838 and Palevsky 2023).

- 840 1. Gather CTD-DO factory-provided calibration coefficients. Before starting the calibration process,
841 ensure no changes to CTD pump or oxygen sensor were made over the course of the cruise. If
842 the CTD pump or oxygen sensor was changed at any point, group data by time before/after the
843 change(s) and apply the following workflow separately to each data grouping to determine the
844 optimal calibration coefficients for each distinct pump and sensor combination.
- 845 2. Process and assemble SBE CTD-DO bottle files. CTD-DO are processed using the Seabird Data
846 Processing Software, creating bottle summary files. File output variables must include a minimum
847 of latitude, longitude, pressure, temperature, conductivity, and dissolved oxygen (volts). We
848 recommend these oxygen voltages are processed with the default hysteresis correction and without
849 the τ_{20} correction. Note, profilers are often equipped with primary and secondary CTD sensors
850 with typically a single oxygen sensor inline with the primary CTD package. Salinity, temperature,
851 and pressure measurements that correspond to the CTD package equipped with the inline oxygen
852 sensor should be used in calibration of the oxygen sensor unless the data is compromised. Ideally,
853 salinity values will have been calibrated with bottle salts.
- 854 3. QA/QC Winkler samples.
- 855 4. Determine calibration coefficients for S_{oc} and E in Equation B1 by applying a non-linear least
856 squares fit to the Winklers collected over the whole cruise while calibration coefficients for A , B ,
857 C , and V_{off} are held constant. Winkler outliers are removed statistically using a non-linear least
858 squares fit until no outliers remain. (Figure ??). Best methods for statistically determining Winkler
859 outliers will depend on the number of Winklers.
- 860 5. Check residuals (Winkler concentration – CTD-DO concentration) as a function of pressure,
861 temperature, DO concentration, and cast number (Figure B1). With outliers removed, residuals
862 between CTD values and water sample values are then examined as a function of pressure,

temperature, oxygen concentration, and cast number (cruise time). An examination of the residuals as a function of cast number is beneficial for 1) identifying episodic events resulting in abrupt changes in Soc values, and 2) determining potential drift in Soc over the course of the cruise. After examining the residuals, cast numbers can be broken into groups if necessary to minimize the residuals with an attempt to limit the number of groups used per cruise. New calibration coefficients are then determined for each group. If a linear drift as a function of time or cast number is determined for a group, a linear correction of the Soc drift can be applied to the group while keeping other coefficients constant.

6. Evaluate possible relationship between S_{OC} term and cruise time/cast number. (Figure B2). Assuming the constant E term determined in Step 4, calculate the S_{OC} term for each Winkler value by rearranging Equation B1. Next, calculate the mean S_{OC} terms for Winklers grouped by cast number and determine if S_{OC} is drifting over cruise time or number of casts. For AR69-01, S_{OC} terms were found to linearly drift over the course of the cruise; therefore we determined that a SOC term that depends on cast number would further minimize residuals (Winklers – CTD-DO Value).
7. Equation B1 is modified to include an S_{OC} term with a linear drift as a function of cast number, replacing Soc as a function of cast number as:

$$S_{OC_{drift}} = F * C + S_{OC_1}, \quad (\text{B2})$$

Where C is the cruise cast number, S_{OC_1} is the calibration slope for the first cruise cast, and F is the rate of S_{OC} change per cast number.

A nonlinear functional fit including the time-dependent/cast-dependent S_{OC} is then fit to the group determining coefficients for E , S_{OC_1} , and F while holding A , B , C , and V_{off} constant (Figure ??).

8. Check residuals (Winkler concentration – CTD-DO concentration) as a function of pressure, temperature, concentration, and cast number (Figure B3). After iterative fitting and removal of outliers, there should no longer be a linear dependence between residuals and cast number.
9. Process the CTD-DO casts in SBE Processing Software to output oxygen values in engineering units of voltages using the default hysteresis correction. Note, oxygen (voltages) will be converted to scientific units ($\mu\text{mol/kg}$) later in this processing pipeline using the SBE calibration equation with Winkler-optimized calibration coefficients.
10. Determine the time response delay of the electrode. Oxygen sensors do not measure oxygen instantaneously and profiles need to be corrected for this time delay. The SBE 43 time delay is due to the response time of the oxygen sensor, the transit time of the water sample in the pumped plumbing line, and the physical misalignment of sensors in depth (Sea-Bird Scientific University Module 27). The delay correction requires iterative application of different oxygen sensor time

897 alignments with typical delays of +3 to +7 seconds relative to the pressure sensor. We have found
898 that visual inspection of oxygen (voltage) in both pressure and temperature space (Figure B4)
899 allows for application of different sensor alignments while ensuring that oxygen sensor misalignment
900 between downcasts and upcasts is not due to changes in hydrographic properties over the course
901 of the cast (Figure B5).

- 902 11. Process CTD casts with Winkler-optimized oxygen calibration coefficients using Equations B1 and
903 B2. Convert CTD-DO data from raw data to engineering units with application of the hysteresis
904 correction. Apply a user-determined oxygen sensor delay of 4 seconds and convert from voltages
905 to oxygen concentrations applying Winkler-optimized calibration coefficients and salinity-calibrated
906 CTD measurements to the sea-bird oxygen calibration equation with a cast-varying SOC term.
- 907 12. Validate calibration. We have found that checking the CTD-DO calibration against oxygen values
908 from deep, relatively stable water masses using historical or recently collected data that overlaps in
909 space or time provides a good check on the quality of CTD-DO calibration.

- 910 Aanderaa Data Instruments (2018). *Aanderaa Oxygen Optodes: Best Practices for Maintaining High*
911 *Data Quality*. en. Accepted: 2020-06-25T20:40:36Z. DOI: 10.25607/0BP-868.
- 912 Atamanchuk, D., J. Koelling, U. Send, and D. W. R. Wallace (Mar. 2020). "Rapid transfer of oxygen
913 to the deep ocean mediated by bubbles". en. In: *Nature Geoscience* 13.3. Number: 3 Publisher:
914 Nature Publishing Group, pp. 232–237. ISSN: 1752-0908. DOI: 10.1038/s41561-020-0532-2.
- 915 Atamanchuk, Dariia, Jaime Palter, Hilary Palevsky, Isabela Le Bras, Jannes Koelling, and David Nicholson
916 (Dec. 2021). "Linking Oxygen and Carbon Uptake with the Meridional Overturning Circulation
917 Using a Transport Mooring Array". In: *Oceanography*, pp. 9–9. ISSN: 10428275. DOI: 10.5670/
918 oceanog.2021.supplement.02-03.
- 919 Atkinson, M. J., F. I. M. Thomas, and N. Larson (Dec. 1996). "Effects of Pressure on Oxygen Sensors".
920 EN. In: *Journal of Atmospheric and Oceanic Technology* 13.6. Publisher: American Meteorological
921 Society Section: Journal of Atmospheric and Oceanic Technology, pp. 1267–1274. ISSN: 0739-0572,
922 1520-0426. DOI: 10.1175/1520-0426(1996)013<1267:EPOOOS>2.0.CO;2.
- 923 Berx, Bee, Stuart Cunningham, Wilken-Jon von Appen, Dariia Atamanchuk, Peter Brown, Neil Fraser,
924 Johannes Hahn, Kerstin Jochumsen, Claire Johnson, Femke de Jong, Johannes Karstensen, Brian
925 King, Matthias Lankhorst, Karin M. H. Larsen, Elaine McDonagh, Martin Moritz, and Igor Yashayaev
926 (Mar. 2019). *Report on the observational potential of the TMAs*. en. Report. Num Pages: 35.
927 AtlantOS. DOI: 10.3289/atlantos_d3.18.
- 928 Bittig, Henry C., Björn Fiedler, Peer Fietzek, and Arne Körtzinger (Dec. 2015). "Pressure Response of
929 Aanderaa and Sea-Bird Oxygen Optodes". EN. In: *Journal of Atmospheric and Oceanic Technology*
930 32.12. Publisher: American Meteorological Society Section: Journal of Atmospheric and Oceanic
931 Technology, pp. 2305–2317. ISSN: 0739-0572, 1520-0426. DOI: 10.1175/JTECH-D-15-0108.1.
- 932 Bittig, Henry C. and Arne Körtzinger (Aug. 2015). "Tackling Oxygen Optode Drift: Near-Surface and
933 In-Air Oxygen Optode Measurements on a Float Provide an Accurate in Situ Reference". EN.
934 In: *Journal of Atmospheric and Oceanic Technology* 32.8. Publisher: American Meteorological

- 935 Society Section: Journal of Atmospheric and Oceanic Technology, pp. 1536–1543. ISSN: 0739-0572,
936 1520-0426. DOI: 10.1175/JTECH-D-14-00162.1.
- 937 Bittig, Henry C. and Arne Körtzinger (Jan. 2017). "Technical note: Update on response times, in-air
938 measurements, and in situ drift for oxygen optodes on profiling platforms". English. In: *Ocean Science*
939 13.1. Publisher: Copernicus GmbH, pp. 1–11. ISSN: 1812-0784. DOI: 10.5194/os-13-1-2017.
- 940 Bittig, Henry C., Arne Körtzinger, Ken Johnson, Herve Claustre, Steve Emerson, Katja Fennel, Hernan
941 Garcia, Denis Gilbert, Nicolas Gruber, Dong-Jin Kang, Wajih Naqvi, Satya Prakash, Steven Riser,
942 Virginie Thierry, Bronte Tilbrook, Hiroshi Uchida, Osvaldo Ulloa, and Xiaogang Xing (Apr. 2018a).
943 "SCOR WG 142: Quality Control Procedures for Oxygen and Other Biogeochemical Sensors on
944 Floats and Gliders. Recommendations on the conversion between oxygen quantities for Bio-Argo
945 floats and other autonomous sensor platforms". en. In.
- 946 Bittig, Henry C., Arne Körtzinger, Craig Neill, Eikbert van Ooijen, Joshua N. Plant, Johannes Hahn,
947 Kenneth S. Johnson, Bo Yang, and Steven R. Emerson (2018b). "Oxygen Optode Sensors: Principle,
948 Characterization, Calibration, and Application in the Ocean". In: *Frontiers in Marine Science* 4.
949 ISSN: 2296-7745.
- 950 Bushinsky, Seth M. and Steven Emerson (Sept. 2013). "A method for in-situ calibration of Aanderaa
951 oxygen sensors on surface moorings". In: *Marine Chemistry* 155, pp. 22–28. ISSN: 0304-4203. DOI:
952 10.1016/j.marchem.2013.05.001.
- 953 Bushinsky, Seth M., Steven R. Emerson, Stephen C. Riser, and Dana D. Swift (2016). "Accurate
954 oxygen measurements on modified Argo floats using in situ air calibrations". en. In: *Limnology and*
955 *Oceanography: Methods* 14.8. eprint: <https://onlinelibrary.wiley.com/doi/pdf/10.1002/lom3.10107>,
956 pp. 491–505. ISSN: 1541-5856. DOI: 10.1002/lom3.10107.
- 957 Cheung, William W. L., Jorge L. Sarmiento, John Dunne, Thomas L. Frölicher, Vicky W. Y. Lam, M. L.
958 Deng Palomares, Reg Watson, and Daniel Pauly (Mar. 2013). "Shrinking of fishes exacerbates
959 impacts of global ocean changes on marine ecosystems". en. In: *Nature Climate Change* 3.3.
960 Number: 3 Publisher: Nature Publishing Group, pp. 254–258. ISSN: 1758-6798. DOI: 10.1038/
961 nclimate1691.
- 962 D'Asaro, Eric A. and Craig McNeil (Aug. 2013). "Calibration and Stability of Oxygen Sensors on
963 Autonomous Floats". EN. In: *Journal of Atmospheric and Oceanic Technology* 30.8. Publisher:
964 American Meteorological Society Section: Journal of Atmospheric and Oceanic Technology, pp. 1896–
965 1906. ISSN: 0739-0572, 1520-0426. DOI: 10.1175/JTECH-D-12-00222.1.
- 966 Deutsch, Curtis, Aaron Ferrel, Brad Seibel, Hans-Otto Pörtner, and Raymond B. Huey (June 2015).
967 "Climate change tightens a metabolic constraint on marine habitats". In: *Science* 348.6239. Publisher:
968 American Association for the Advancement of Science, pp. 1132–1135. DOI: 10.1126/science.
969 aaa1605.
- 970 Diaz, Robert J. and Rutger Rosenberg (Aug. 2008). "Spreading Dead Zones and Consequences for
971 Marine Ecosystems". In: *Science* 321.5891. Publisher: American Association for the Advancement
972 of Science, pp. 926–929. DOI: 10.1126/science.1156401.

- 973 Dove, Lilian A., Andrew F. Thompson, Dhruv Balwada, and Alison R. Gray (2021). "Observational
974 Evidence of Ventilation Hotspots in the Southern Ocean". en. In: *Journal of Geophysical Research: Oceans* 126.7. eprint: <https://agupubs.onlinelibrary.wiley.com/doi/pdf/10.1029/2021JC017178>,
975 e2021JC017178. ISSN: 2169-9291. DOI: 10.1029/2021JC017178.
- 976
977 Edwards, Bradley, David Murphy, Carol Janzen, and Nordean Larson (May 2010). "Calibration, Response,
978 and Hysteresis in Deep-Sea Dissolved Oxygen Measurements". EN. In: *Journal of Atmospheric and
979 Oceanic Technology* 27.5. Publisher: American Meteorological Society Section: Journal of
980 Atmospheric and Oceanic Technology, pp. 920–931. ISSN: 0739-0572, 1520-0426. DOI: 10.1175/
981 2009JTECH0693.1.
- 982 Emerson, Steven and Charles Stump (Oct. 2010). "Net biological oxygen production in the ocean—II:
983 Remote in situ measurements of O₂ and N₂ in subarctic pacific surface waters". In: *Deep Sea
984 Research Part I: Oceanographic Research Papers* 57.10, pp. 1255–1265. ISSN: 0967-0637. DOI:
985 10.1016/j.dsr.2010.06.001.
- 986 Emerson, Steven, Charles Stump, and David Nicholson (2008). "Net biological oxygen production in the
987 ocean: Remote in situ measurements of O₂ and N₂ in surface waters". en. In: *Global Biogeochemical
988 Cycles* 22.3. eprint: <https://agupubs.onlinelibrary.wiley.com/doi/pdf/10.1029/2007GB003095>.
989 ISSN: 1944-9224. DOI: 10.1029/2007GB003095.
- 990 Fogaren, Kristen E. and Hilary Palevsky (Aug. 2023). *Bottle-calibrated dissolved oxygen profiles from
991 yearly turn-around cruises for the Ocean Observations Initiative (OOI) Irminger Sea Array 2014 –
992 2022*. en. ISBN: 9780646556215. DOI: 10.26008/1912/BC0-DM0.904721.1.
- 993 Hassell, David, Jonathan Gregory, Jon Blower, Bryan N. Lawrence, and Karl E. Taylor (Dec. 2017).
994 "A data model of the Climate and Forecast metadata conventions (CF-1.6) with a software
995 implementation (cf-python v2.1)". English. In: *Geoscientific Model Development* 10.12. Publisher:
996 Copernicus GmbH, pp. 4619–4646. ISSN: 1991-959X. DOI: 10.5194/gmd-10-4619-2017.
- 997 Ito, Takamitsu, Shoshiro Minobe, Matthew C. Long, and Curtis Deutsch (2017). "Upper ocean O₂ trends:
998 1958–2015". en. In: *Geophysical Research Letters* 44.9. eprint: <https://onlinelibrary.wiley.com/doi/pdf/10.1002/2017GL073613>.
999 pp. 4214–4223. ISSN: 1944-8007. DOI: 10.1002/2017GL073613.
- 1000 Jiang, Li-Qing, Denis Pierrot, Rik Wanninkhof, Richard A. Feely, Bronte Tilbrook, Simone Alin, Leticia
1001 Barbero, Robert H. Byrne, Brendan R. Carter, Andrew G. Dickson, Jean-Pierre Gattuso, Dana
1002 Greeley, Mario Hoppema, Matthew P. Humphreys, Johannes Karstensen, Nico Lange, Siv K. Lauvset,
1003 Ernie R. Lewis, Are Olsen, Fiz F. Pérez, Christopher Sabine, Jonathan D. Sharp, Toste Tanhua,
1004 Thomas W. Trull, Anton Velo, Andrew J. Allegra, Paul Barker, Eugene Burger, Wei-Jun Cai, Chen-
1005 Tung A. Chen, Jessica Cross, Hernan Garcia, Jose Martin Hernandez-Ayon, Xinping Hu, Alex Kozyr,
1006 Chris Langdon, Kitack Lee, Joe Salisbury, Zhaohui Aleck Wang, and Liang Xue (Jan. 2022). "Best
1007 Practice Data Standards for Discrete Chemical Oceanographic Observations". English. In: *Frontiers
1008 in Marine Science* 8. Publisher: Frontiers. ISSN: 2296-7745. DOI: 10.3389/fmars.2021.705638.
- 1009 Johnson, Kenneth S., Joshua N. Plant, Stephen C. Riser, and Denis Gilbert (Nov. 2015). "Air Oxygen
1010 Calibration of Oxygen Optodes on a Profiling Float Array". EN. In: *Journal of Atmospheric and
1011 Oceanic Technology* 32.11. Publisher: American Meteorological Society Section: Journal

- of Atmospheric and Oceanic Technology, pp. 2160–2172. ISSN: 0739-0572, 1520-0426. DOI: 10.1175/JTECH-D-15-0101.1.
- Koelling, Jannes, Dariia Atamanchuk, Johannes Karstensen, Patricia Handmann, and Douglas W. R. Wallace (Jan. 2022). “Oxygen export to the deep ocean following Labrador Sea Water formation”. English. In: *Biogeosciences* 19.2. Publisher: Copernicus GmbH, pp. 437–454. ISSN: 1726-4170. DOI: 10.5194/bg-19-437-2022.
- Lakowicz, Joseph R. (1999). *Principles of Fluorescence Spectroscopy*. en. Boston, MA: Springer US. ISBN: 978-1-4757-3063-0 978-1-4757-3061-6. DOI: 10.1007/978-1-4757-3061-6.
- Langdon, C. (2010). “Determination of Dissolved Oxygen in Seawater by Winkler Titration Using The Amperometric Technique.” en. In: Accepted: 2017-11-24T20:21:13Z. DOI: 10.25607/OPB-1350.
- Lévy, Marina, Laure Resplandy, Jaime B. Palter, Damien Couespel, and Zouhair Lachkar (Jan. 2022). “Chapter 13 - The crucial contribution of mixing to present and future ocean oxygen distribution”. en. In: *Ocean Mixing*. Ed. by Michael Meredith and Alberto Naveira Garabato. Elsevier, pp. 329–344. ISBN: 978-0-12-821512-8. DOI: 10.1016/B978-0-12-821512-8.00020-7.
- Lozier, M. S., F. Li, S. Bacon, F. Bahr, A. S. Bower, S. A. Cunningham, M. F. de Jong, L. de Steur, B. deYoung, J. Fischer, S. F. Gary, B. J. W. Greenan, N. P. Holliday, A. Houk, L. Houpert, M. E. Inall, W. E. Johns, H. L. Johnson, C. Johnson, J. Karstensen, G. Koman, I. A. Le Bras, X. Lin, N. Mackay, D. P. Marshall, H. Mercier, M. Oltmanns, R. S. Pickart, A. L. Ramsey, D. Rayner, F. Straneo, V. Thierry, D. J. Torres, R. G. Williams, C. Wilson, J. Yang, I. Yashayaev, and J. Zhao (Feb. 2019). “A sea change in our view of overturning in the subpolar North Atlantic”. In: *Science* 363.6426. Publisher: American Association for the Advancement of Science, pp. 516–521. DOI: 10.1126/science.aau6592.
- Maurer, Tanya L., Joshua N. Plant, and Kenneth S. Johnson (Aug. 2021). “Delayed-Mode Quality Control of Oxygen, Nitrate, and pH Data on SOCCOM Biogeochemical Profiling Floats”. English. In: *Frontiers in Marine Science* 8. Publisher: Frontiers. ISSN: 2296-7745. DOI: 10.3389/fmars.2021.683207.
- Mignot, A., F. D'Ortenzio, V. Taillandier, G. Cossarini, and S. Salon (2019). “Quantifying Observational Errors in Biogeochemical-Argo Oxygen, Nitrate, and Chlorophyll a Concentrations”. en. In: *Geophysical Research Letters* 46.8. eprint: <https://agupubs.onlinelibrary.wiley.com/doi/pdf/10.1029/2018GL080541>, pp. 4330–4337. ISSN: 1944-8007. DOI: 10.1029/2018GL080541.
- Oschlies, Andreas, Peter Brandt, Lothar Stramma, and Sunke Schmidtko (July 2018). “Drivers and mechanisms of ocean deoxygenation”. en. In: *Nature Geoscience* 11.7. Number: 7 Publisher: Nature Publishing Group, pp. 467–473. ISSN: 1752-0908. DOI: 10.1038/s41561-018-0152-2.
- Owens, W. Brechner and Robert C. Millard (May 1985). “A New Algorithm for CTD Oxygen Calibration”. EN. In: *Journal of Physical Oceanography* 15.5. Publisher: American Meteorological Society Section: Journal of Physical Oceanography, pp. 621–631. ISSN: 0022-3670, 1520-0485. DOI: 10.1175/1520-0485(1985)015<0621:ANAFCO>2.0.CO;2.
- Palevsky, Hilary, Sophie Clayton, Dariia Atamanchuk, Roman Battisti, Jennifer Batryn, Annie Bourbonnais, Ellen M. Briggs, Filipa Carvalho, Alison P. Chase, Rachel Eveleth, Rob Fatland, Kristen E. Fogaren,

- 1051 Jonathan Peter Fram, Susan E. Hartman, Isabela Le Bras, Cara C. M. Manning, Joseph A. Needoba,
1052 Merrie Beth Neely, Hilde Oliver, Andrew C. Reed, Jennie E. Rheuban, Christina Schallenberg,
1053 Michael F. Vardaro, Ian Walsh, and Christopher Wingard (2023). *OOI Biogeochemical Sensor*
1054 *Data Best Practices and User Guide. Version 1.1.1. [GOOS ENDORSED PRACTICE]*. en. Report.
1055 Accepted: 2023-08-09T14:56:13Z. Ocean Observatories Initiative, Biogeochemical Sensor Data
1056 Working Group. DOI: 10.25607/0BP-1865.2.
- 1057 Palter, Jaime B. and David S. Trossman (2018). "The Sensitivity of Future Ocean Oxygen to Changes in
1058 Ocean Circulation". en. In: *Global Biogeochemical Cycles* 32.5. _eprint: <https://onlinelibrary.wiley.com/doi/pdf/10.10>
1059 pp. 738–751. ISSN: 1944-9224. DOI: 10.1002/2017GB005777.
- 1060 Ren, Alice S., Daniel L. Rudnick, and Alistair Twombly (Dec. 2023). "Drift Characteristics of Sea-Bird
1061 Dissolved Oxygen Optode Sensors". EN. In: *Journal of Atmospheric and Oceanic Technology*
1062 40.12. Publisher: American Meteorological Society Section: Journal of Atmospheric and Oceanic
1063 Technology, pp. 1645–1656. ISSN: 0739-0572, 1520-0426. DOI: 10.1175/JTECH-D-22-0103.1.
- 1064 SeaBird Electronics (Sept. 2023). *SBE 63 Optical Dissolved Oxygen Sensor User Manual*.
- 1065 Stendardo, I. and N. Gruber (2012). "Oxygen trends over five decades in the North Atlantic". en. In: *Jour-*
1066 *nal of Geophysical Research: Oceans* 117.C11. _eprint: <https://onlinelibrary.wiley.com/doi/pdf/10.1029/2012JC00790>
1067 ISSN: 2156-2202. DOI: 10.1029/2012JC007909.
- 1068 Takeshita, Yuichiro, Todd R. Martz, Kenneth S. Johnson, Josh N. Plant, Denis Gilbert, Stephen C.
1069 Riser, Craig Neill, and Bronte Tilbrook (2013). "A climatology-based quality control procedure
1070 for profiling float oxygen data". en. In: *Journal of Geophysical Research: Oceans* 118.10. _eprint:
1071 <https://agupubs.onlinelibrary.wiley.com/doi/pdf/10.1002/jgrc.20399>, pp. 5640–5650. ISSN: 2169-
1072 9291. DOI: 10.1002/jgrc.20399.
- 1073 Tengberg, Anders, Jostein Hovdenes, Henrik Johan Andersson, Olivier Brocandel, Robert Diaz, David
1074 Hebert, Tony Arnerich, Christian Huber, Arne Körtzinger, Alexis Khripounoff, Francisco Rey, Christer
1075 Rönning, Jens Schimanski, Stefan Sommer, and Achim Stanelmayer (2006). "Evaluation of a
1076 lifetime-based optode to measure oxygen in aquatic systems". en. In: *Limnology and Oceanography:*
1077 *Methods* 4.2. _eprint: <https://onlinelibrary.wiley.com/doi/pdf/10.4319/lom.2006.4.7>, pp. 7–17.
1078 ISSN: 1541-5856. DOI: 10.4319/lom.2006.4.7.
- 1079 Thierry, Virginie, Henry C. Bittig, Denis Gilbert, Taiyo Kobayashi, Sato Kanako, and Claudia Schmid
1080 (Apr. 2022). "Processing Argo oxygen data at the DAC level". en. In.
- 1081 Thierry, Virginie, Henry C. Bittig, and The Argo-Bgc Team (Feb. 2021). "Argo quality control manual
1082 for dissolved oxygen concentration". en. In.
- 1083 Thomas, Leif N. and Terrence M. Joyce (Feb. 2010). "Subduction on the Northern and Southern
1084 Flanks of the Gulf Stream". EN. In: *Journal of Physical Oceanography* 40.2. Publisher: American
1085 Meteorological Society Section: Journal of Physical Oceanography, pp. 429–438. ISSN: 0022-3670,
1086 1520-0485. DOI: 10.1175/2009JP04187.1.
- 1087 Uchida, Hiroshi, G. C. Johnson, and K. E. McTaggart (2010). "CTD Oxygen Sensor Calibration
1088 Procedures". en. In: Accepted: 2017-11-24T12:04:56Z. DOI: 10.25607/0BP-1344.

- 1089 Uchida, Hiroshi, Takeshi Kawano, Ikuo Kaneko, and Masao Fukasawa (Dec. 2008). "In Situ Calibration
1090 of Optode-Based Oxygen Sensors". EN. In: *Journal of Atmospheric and Oceanic Technology*
1091 25.12. Publisher: American Meteorological Society Section: Journal of Atmospheric and Oceanic
1092 Technology, pp. 2271–2281. ISSN: 0739-0572, 1520-0426. DOI: 10.1175/2008JTECH0549.1.
- 1093 Wilkinson, Mark D., Michel Dumontier, IJsbrand Jan Aalbersberg, Gabrielle Appleton, Myles Axton,
1094 Arie Baak, Niklas Blomberg, Jan-Willem Boiten, Luiz Bonino da Silva Santos, Philip E. Bourne,
1095 Jildau Bouwman, Anthony J. Brookes, Tim Clark, Mercè Crosas, Ingrid Dillo, Olivier Dumon,
1096 Scott Edmunds, Chris T. Evelo, Richard Finkers, Alejandra Gonzalez-Beltran, Alasdair J. G. Gray,
1097 Paul Groth, Carole Goble, Jeffrey S. Grethe, Jaap Heringa, Peter A. C. 't Hoen, Rob Hooft, Tobias
1098 Kuhn, Ruben Kok, Joost Kok, Scott J. Lusher, Maryann E. Martone, Albert Mons, Abel L. Packer,
1099 Bengt Persson, Philippe Rocca-Serra, Marco Roos, Rene van Schaik, Susanna-Assunta Sansone,
1100 Erik Schultes, Thierry Sengstag, Ted Slater, George Strawn, Morris A. Swertz, Mark Thompson,
1101 Johan van der Lei, Erik van Mulligen, Jan Velterop, Andra Waagmeester, Peter Wittenburg,
1102 Katherine Wolstencroft, Jun Zhao, and Barend Mons (Mar. 2016). "The FAIR Guiding Principles
1103 for scientific data management and stewardship". en. In: *Scientific Data* 3.1. Number: 1 Publisher:
1104 Nature Publishing Group, p. 160018. ISSN: 2052-4463. DOI: 10.1038/sdata.2016.18.
- 1105 Winkler (1888). "The determination of dissolved oxygen". In: *Ber. Dtsch. Chem. Ges.* 21, pp. 2, 843–2,
1106 846.
- 1107 Wolf, Mitchell K., Roberta C. Hamme, Denis Gilbert, Igor Yashayaev, and Virginie Thierry (2018). "Oxygen
1108 Saturation Surrounding Deep Water Formation Events in the Labrador Sea From Argo-O2 Data". en.
1109 In: *Global Biogeochemical Cycles* 32.4. eprint: <https://agupubs.onlinelibrary.wiley.com/doi/pdf/10.1002/2017GB005829>.
1110 pp. 635–653. ISSN: 1944-9224. DOI: 10.1002/2017GB005829.
- 1111 Zhang, Jia-Zhong, George Berberian, and Rik Wanninkhof (Sept. 2002). "Long-term storage of natural
1112 water samples for dissolved oxygen determination". In: *Water Research* 36.16, pp. 4165–4168. ISSN:
1113 0043-1354. DOI: 10.1016/S0043-1354(02)00093-3.

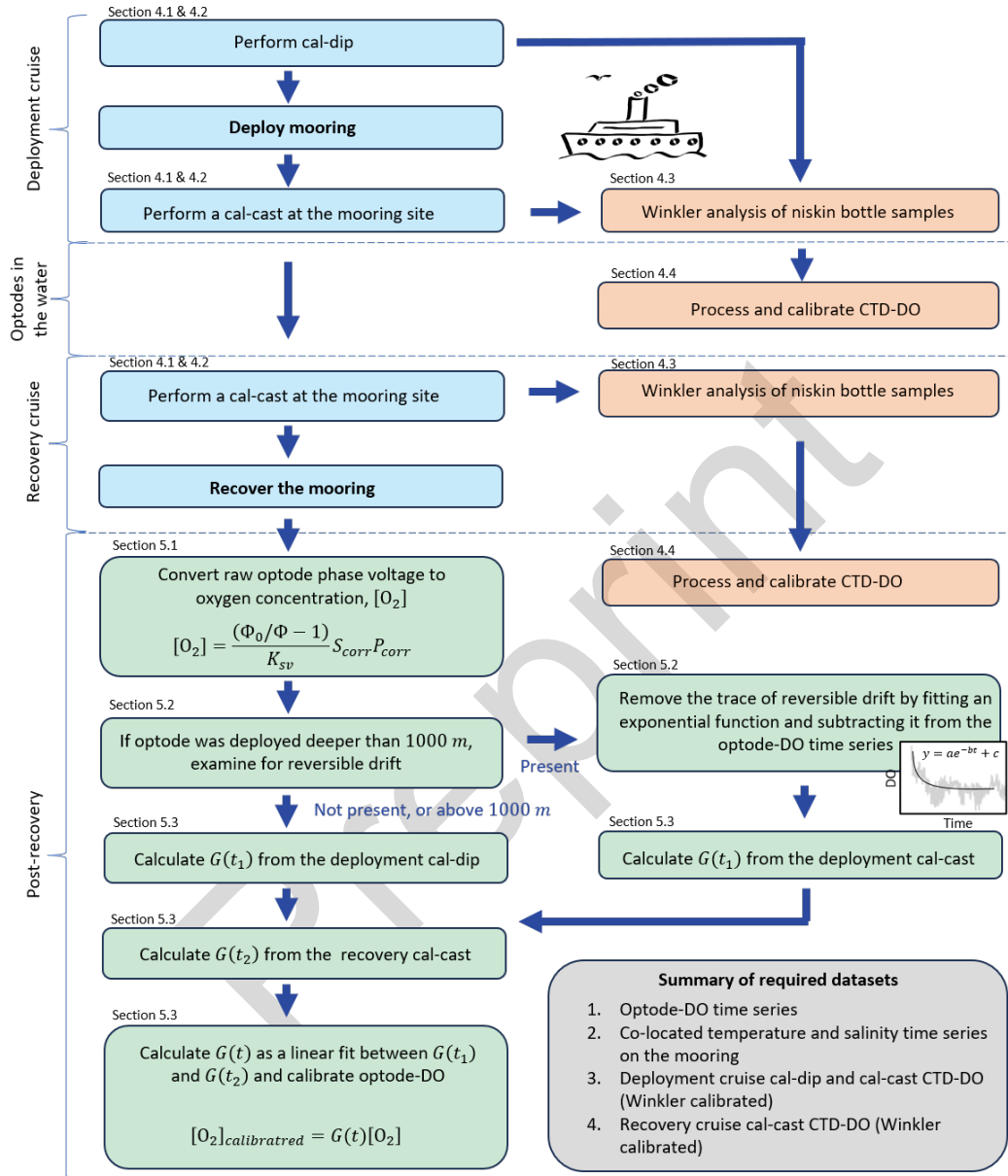


Figure 1: Flowchart summarizing the key protocols described in this paper, which are color coded and grouped as: a) (blue) cruise activities: the deployment and recovery of the moored optodes (Section 3), along with the collection of necessary CTD-DO profiles (Section 4.2 and 4.1) b) (orange) CTD-DO processing and calibration activities: Winkler analysis (Section 4.3) and calibration of CTD-DO using Winklers (Section 4.4), and c) (green) optode processing and calibration activities: the processing (Section 5.1) and drift correction (Sections 5.2 and 5.3) of optode data. Term definitions may be found in Table 1.

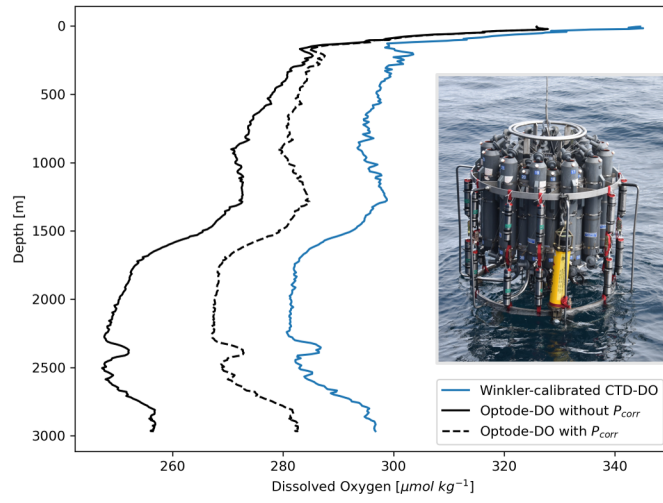


Figure 2: An example cal-dip profile illustrating the pressure-dependent low-bias in optode-DO (solid black line) relative to Winkler-calibrated CTD-DO (blue line) evident when the P_{corr} coefficient in Equation 1 has not been applied. Application of P_{corr} removes the pressure-dependent bias (dotted black line). The inset photo shows an example of a cal-dip, where the optodes are strapped to the frame of the CTD profiler.

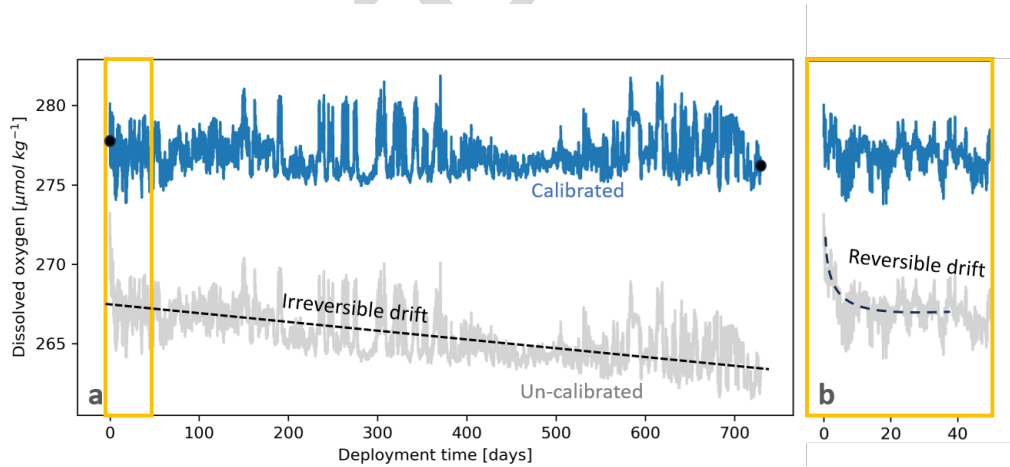


Figure 3: Examples of how a) irreversible and b) reversible drift appear in uncalibrated moored optode-DO time series. The time series shown here was collected over a 2-year deployment period at 2022 m depth at OSNAP Station K10, and exhibits both types of drift. The black dots near the start and end of the time series in Panel (a) indicate the calibration points derived from CTD-DO. Panel (b) zooms in on the first 50 days, outlined in the yellow box in panel a.

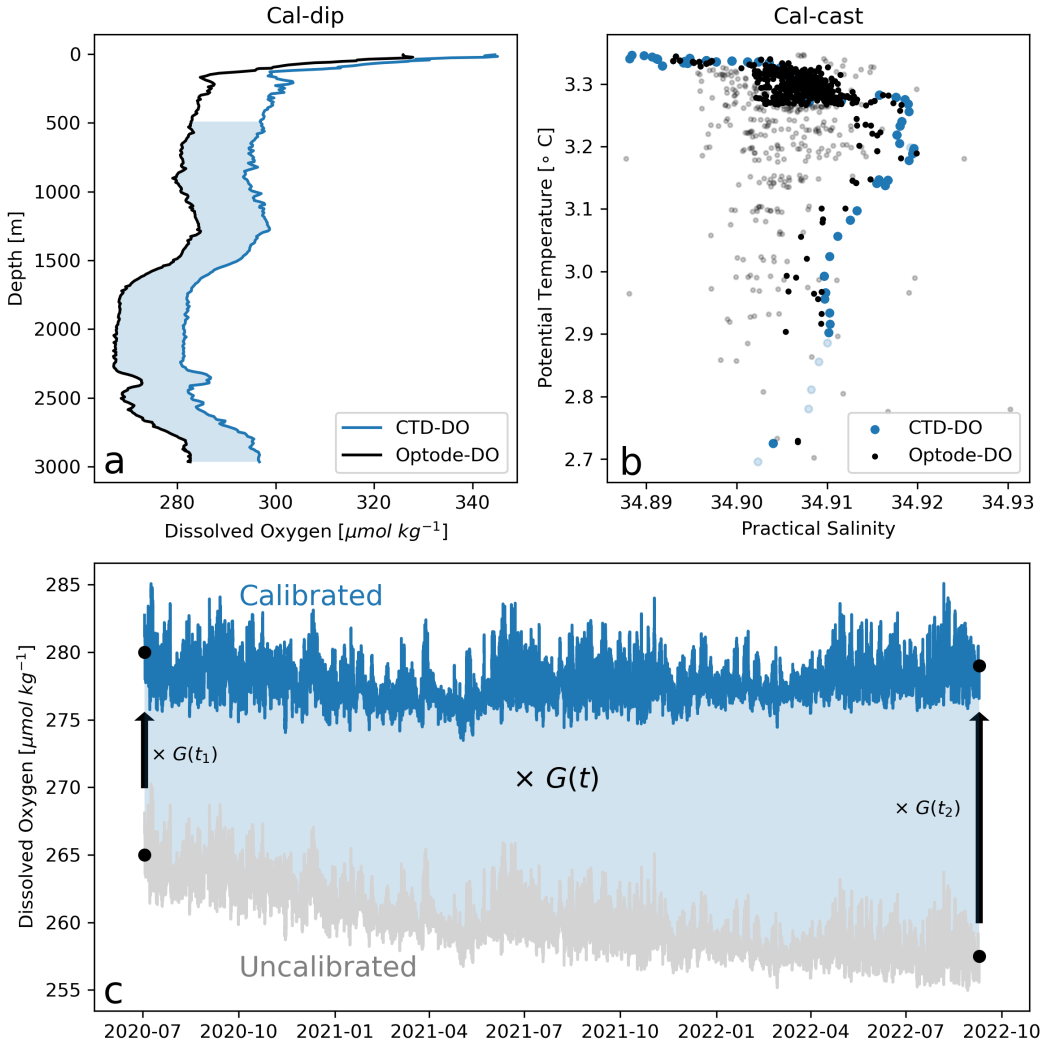


Figure 4: Calibration of optode-DO. a) Calculation of $G(t_1)$ or $G(t_2)$ (Equation 5) from cal-dip profiles of pressure-corrected (P_{corr}) optode-DO and Winkler-calibrated CTD-DO. Here, data shallower than 500 m is excluded due to high upper-ocean variability and possible hysteresis in the optode relative to the electrode. b) Each cal-cast optode-DO data point is matched with any cal-cast CTD-DO data point that falls within specified temperature, salinity, and pressure thresholds in blue and black, respectively. Data points that do not match within these criteria are shown in grey and light blue, respectively. Optode-DO are within ± 5 days of the cal-cast date. c) A conceptual depiction of how $G(t_1)$ and $G(t_2)$ are used in calibration to "pin" the two ends of the uncalibrated optode-DO time series. This is done by multiplying the uncalibrated optode-DO by $G(t)$, a linear fit between $G(t_1)$ and $G(t_2)$.

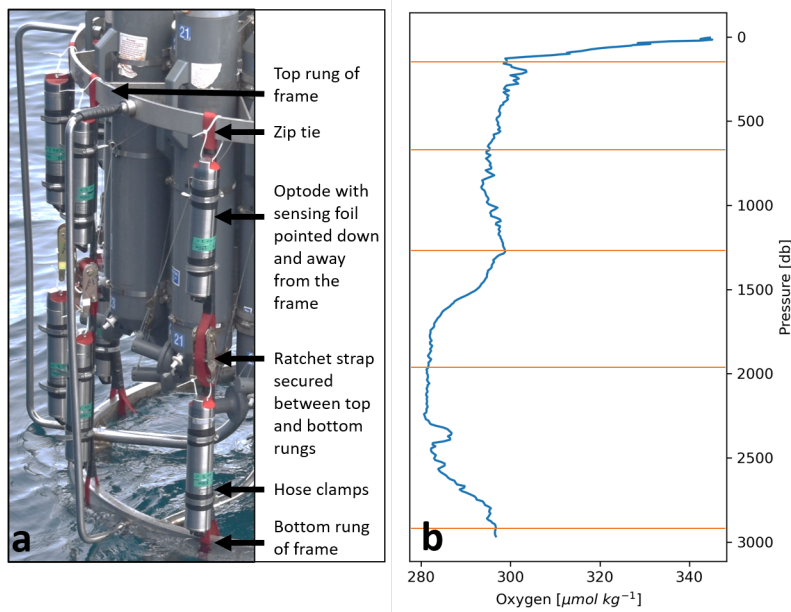


Figure 5: CTD-DO setup and deployment. a) An example of how optodes are strapped to the frame of the CTD-profiler in order to perform a calibration "dip" cast, or "cal-dip". b) An example of a CTD-DO profile with depths (dashed orange lines) selected for upcast niskin bottle sampling for Winkler analysis.

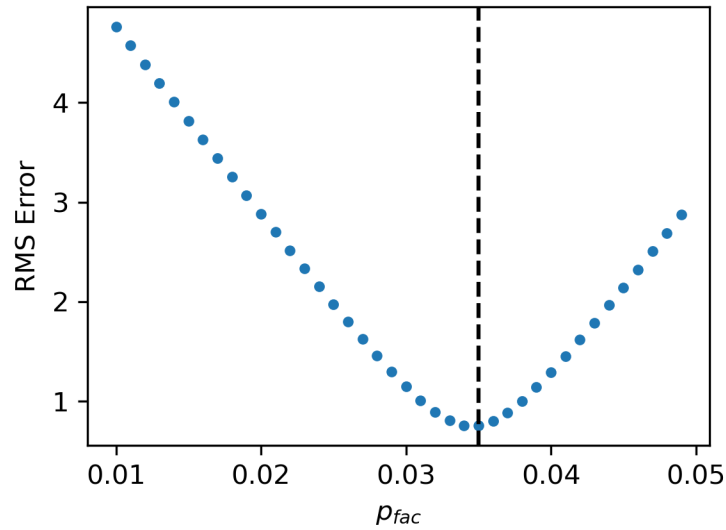


Figure 6: An example of the root-square-mean (RMS) error between the cal-dip CTD-DO and optode-DO profiles using values of p_{fac} in Equation 6d ranging from 0.01 to 0.05. The value of p_{fac} that minimizes RMS error ($p_{fac} = 0.0349$) is the optimal p_{fac} for this particular optode.

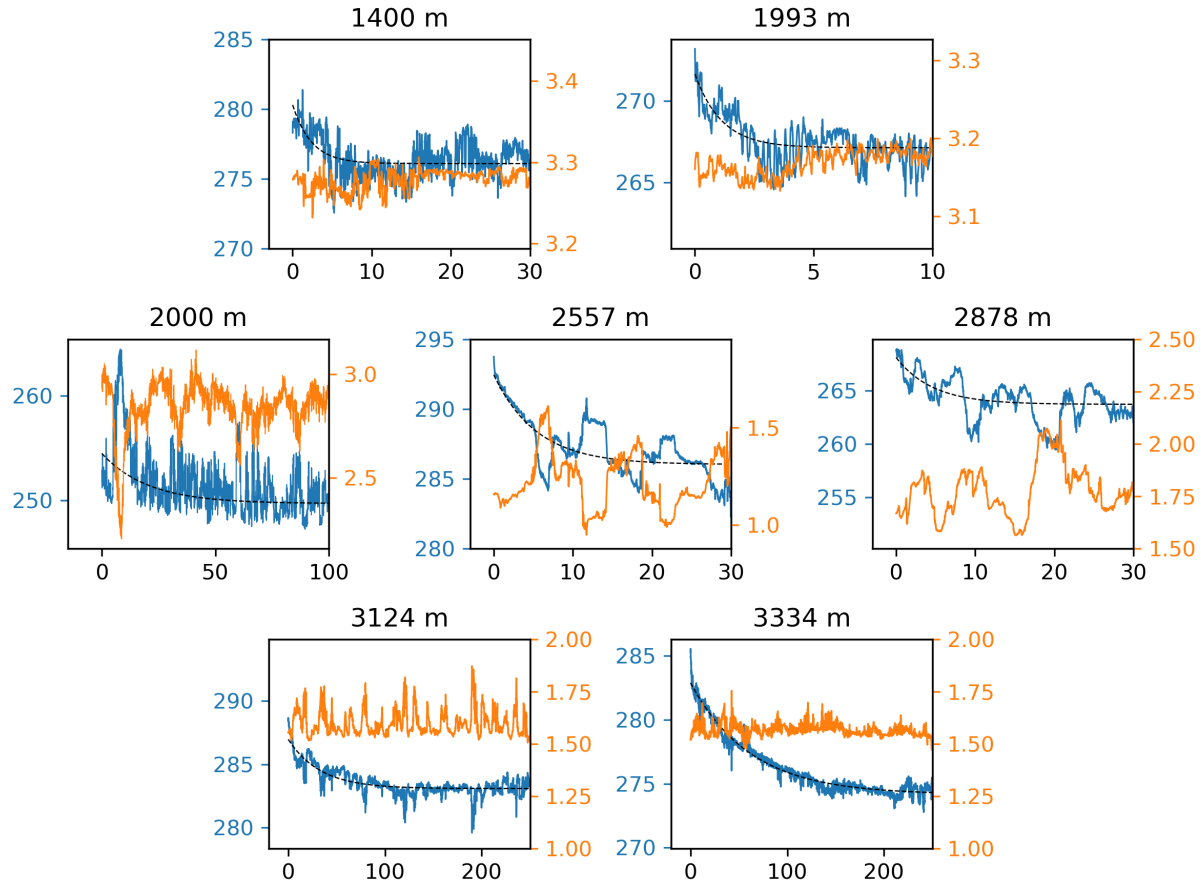


Figure 7: Reversible drift in 7 of 24 GOHSNAP optodes deployed at depths greater than 1000 m. In all subplots, the horizontal axis is time in days since deployment and the vertical axis is dissolved oxygen (DO) in $\mu\text{mol kg}^{-1}$ in blue and potential temperature in $^{\circ}\text{C}$ in orange. In each panel, an exponential decay is clear in the optode-DO time series but not in the co-located temperature time series. Dashed lines show the least-squares fit to the optode-DO. For time constants and magnitudes of the fitted drifts, see Table 2.

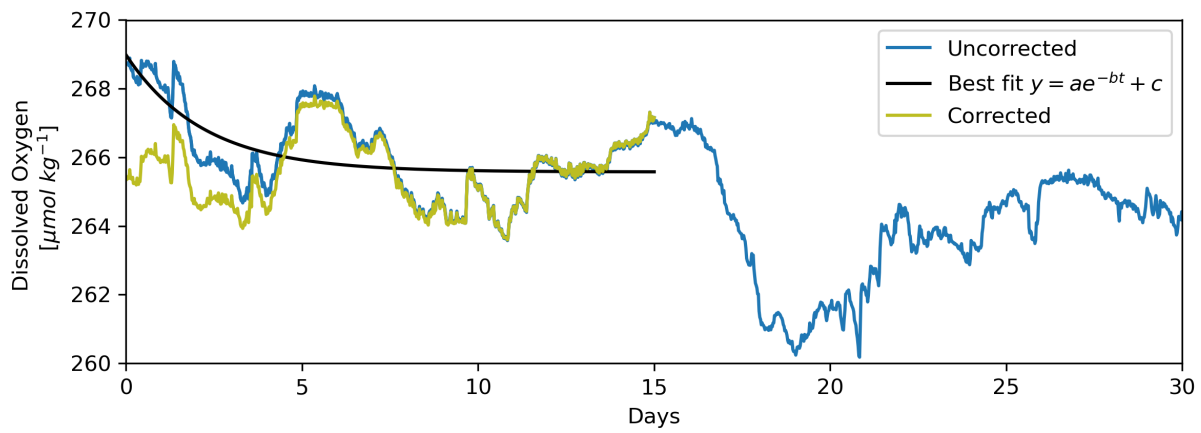


Figure 8: Removal of reversible drift via fitting and subtraction of an exponential function. The "Corrected" (yellow) time series results from the subtraction of the least-squares fit exponential function (without c , i.e., ae^{-bt}) from the "Uncorrected" (blue) time series. This example from the K9 mooring (western Labrador Sea) at a depth of 2878 m exhibits "fast" reversible drift, which occurs in the first days to weeks of deployment (also shown in right-most panel of middle row in Figure 7).

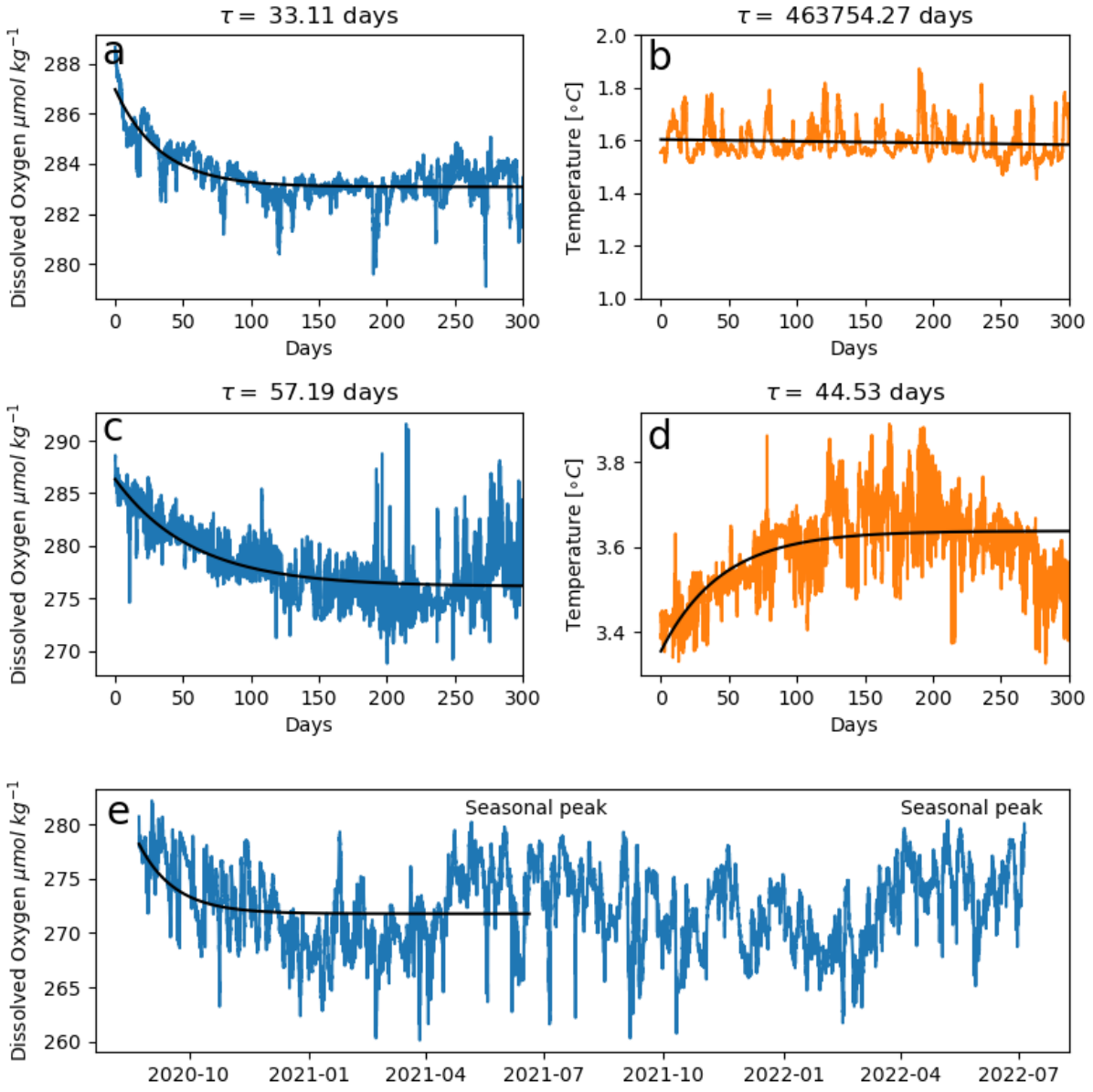


Figure 9: Determination of the presence or absence of reversible drift in three example optodes following the criteria outlined in Section 5.2. In the first optode (the same optode at 3124 m shown in Figure 7), an optimal fit is found for (a) the DO time series but not the (b) co-located temperature time series, suggesting reversible drift is present. In the second optode, an optimal fit is found for both the DO (c) and temperature (d) time series, and their similar exponential decay time constants (τ) suggest that reversible drift is not present. (e) Shows an example of an optode-DO time series that was determined not to exhibit reversible drift even though a fit was found for the optode-DO time series and not in the temperature time series (latter not shown). In addition to failing criterion 3(d)iii for reversible drift, the initial decay here appears to be a real decline in DO that is part of a regular seasonal cycle of peaks and declines at this site.

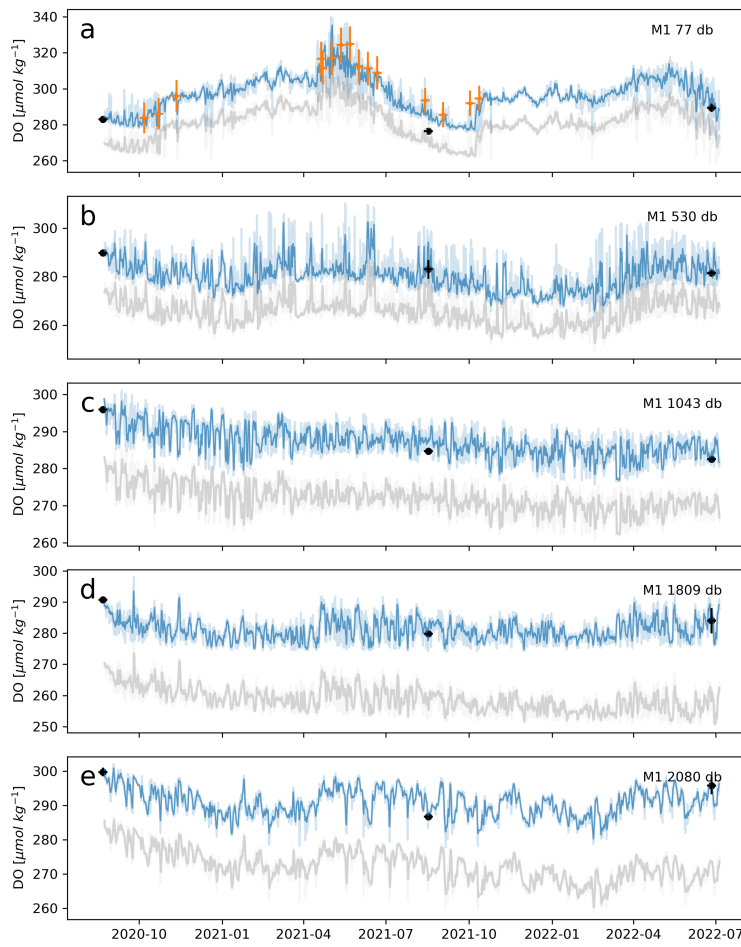


Figure 10: 1-day-averaged, calibrated optode-DO (blue time series) from OSNAP Mooring M1 in the western Irminger Sea, validated against available delayed-mode BGC-Argo-DO (orange) and Winkler-calibrated CTD-DO (black) measurements. The 1-day-averaged uncalibrated optode-DO is shown in grey. Underlaid light blue and light grey time series show the full, un-averaged calibrated and uncalibrated time series, respectively. The CTD-DO data points are from the deployment and recovery cruise cal-casts and represent the average DO from the portion of each profile that matches the optode within specified temperature, salinity, and pressure thresholds. In optode-DO time series without reversible drift, the deployment cruise cal-cast was not used in the calibration and therefore serves as an external validation point. The fortuitously-collected mid-deployment CTD-DO data points were also not used in the calibration and serve as external validation points. The BGC-Argo-DO data points represent data from individual profiles across a number of floats that have been matched to the optode using the same temperature, salinity, and pressure criteria as with CTD-DO, within a 100km radius of the mooring site. Horizontal error bars on all data points indicate the +/- 5 day period over which the water mass matchup was performed. Vertical error bars on the cal-cast are the standard deviation of the CTD-DO within the water mass matching criteria. Vertical error bars on the BGC-ARGO-DO indicate the error reported within the data file. Note that BGC-ARGO-DO profiles that match one depth/optode on a mooring will typically match multiple other depths/optodes on that same mooring. In this case, only the near-surface water mass at the mooring site matched with those sampled by the Argo floats, with spatial variability at deeper depths yielding no Argo-optode matchups within the chosen distance, temperature, salinity, and pressure thresholds.

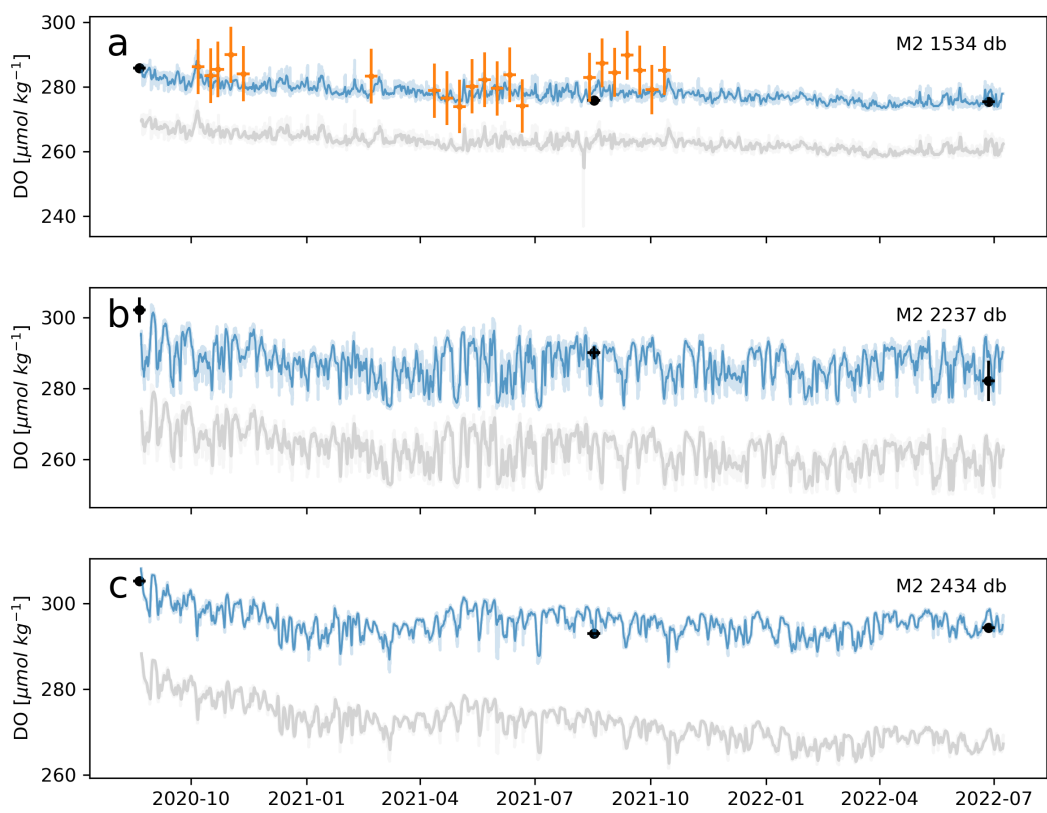


Figure 11: Same as in Figure 10 but for optodes on OSNAP Mooring M2.

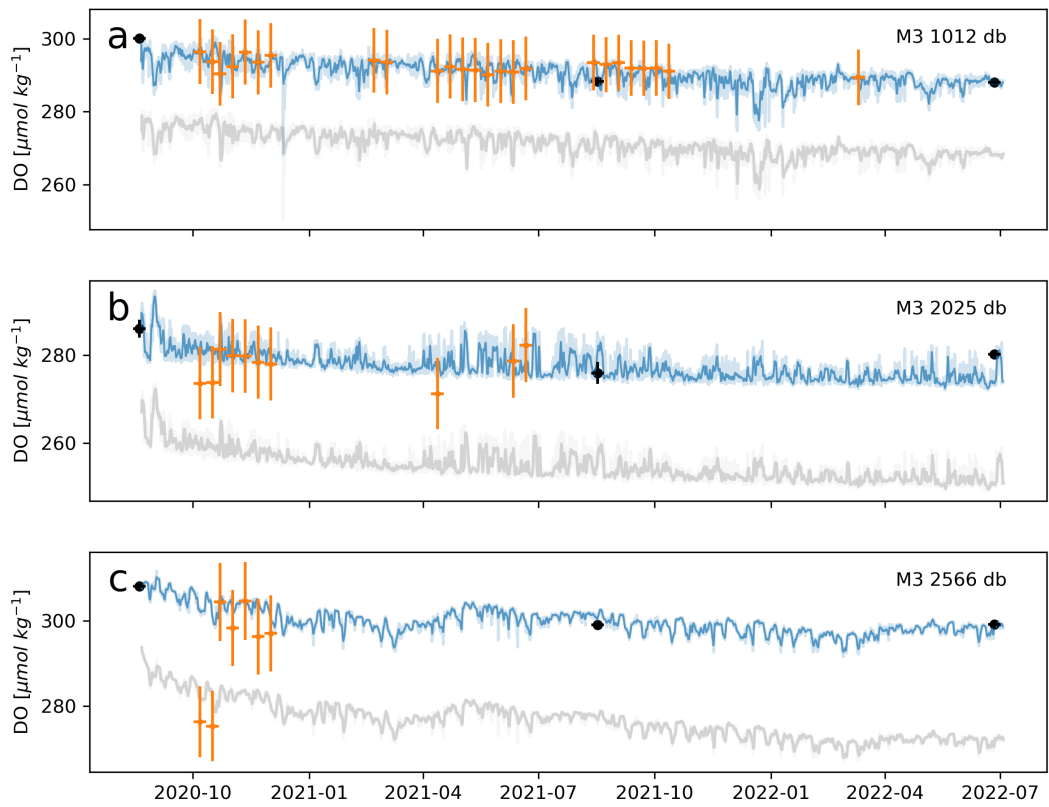


Figure 12: Same as in Figure 10 but for optodes on OSNAP Mooring M3. Note that Argos typically sample only to depths less than 2000 m, but data shown here were collected by a "Deep-Arvor float", capable of sampling as deep as 4000 m. In panel c, the two BGC-Argo-DO points that appear much lower than the remaining points were from a separate float with a separate calibration procedure. As values of $\sim 250/\mu\text{mol kg}^{-1}$ are anomalously low for this region, the discrepancy may indicate an issue with the calibration of that particular float.

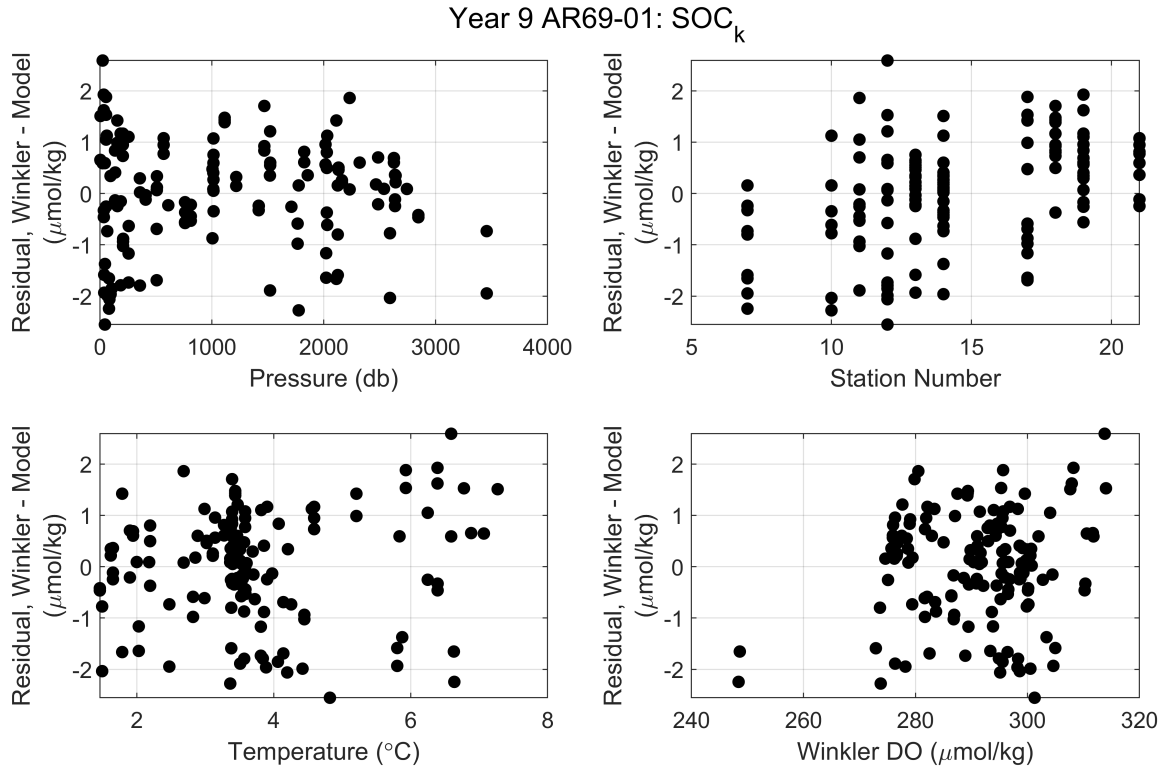


Figure B1: Oxygen residuals (Winkler values – CTD values, $\mu\text{mol}/\text{kg}$) for calibrated CTD-DO sensor as a function of pressure (db), time (d), temperature ($^{\circ}\text{C}$) and Winkler-determined oxygen concentration ($\mu\text{mol}/\text{kg}$). Model determined outliers have been removed.

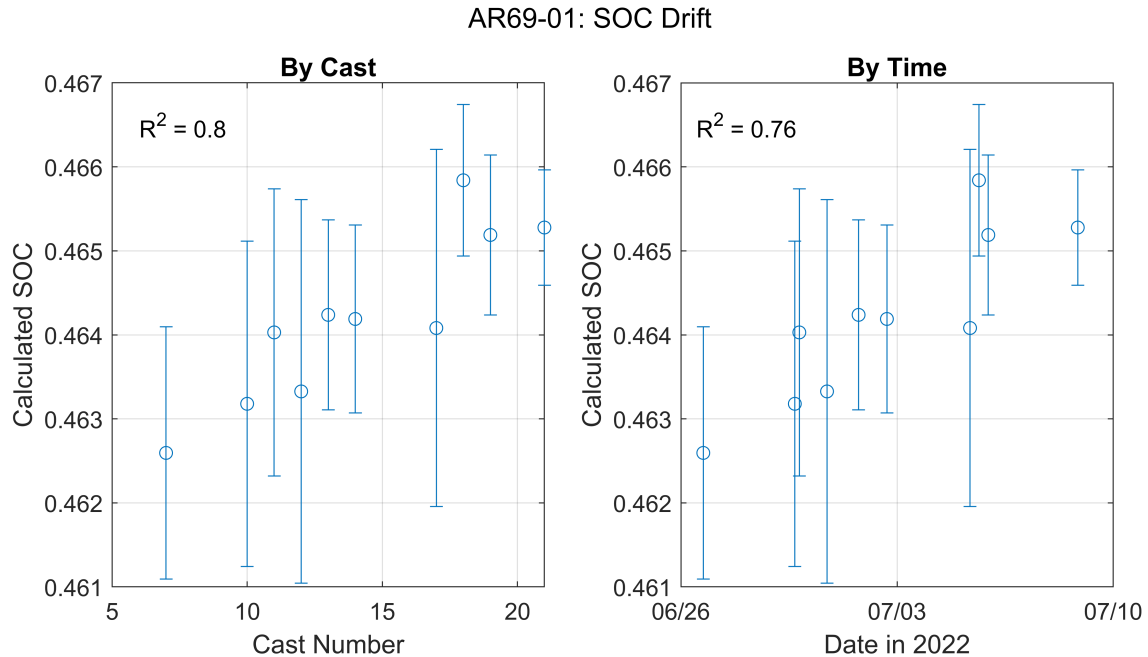


Figure B2: Calculated S_{oc} term as a function of cast number (left panel) or cruise time (right panel). R^2 values are shown on plots.

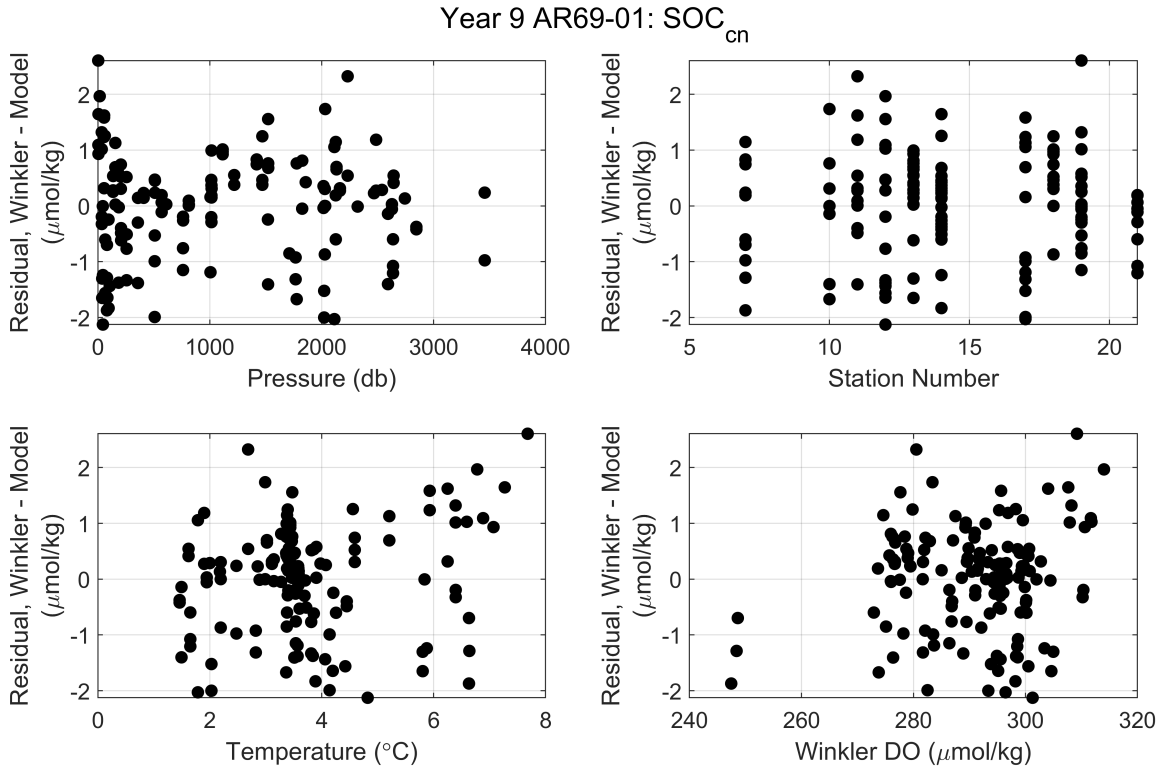


Figure B3: Oxygen residuals (Winkler values – CTD values, $\mu\text{mol}/\text{kg}$) for calibrated CTD-DO sensor as a function of pressure (db), time (d), temperature ($^{\circ}\text{C}$) and Winkler-determined oxygen concentration ($\mu\text{mol}/\text{kg}$). Model determined outliers have been removed.

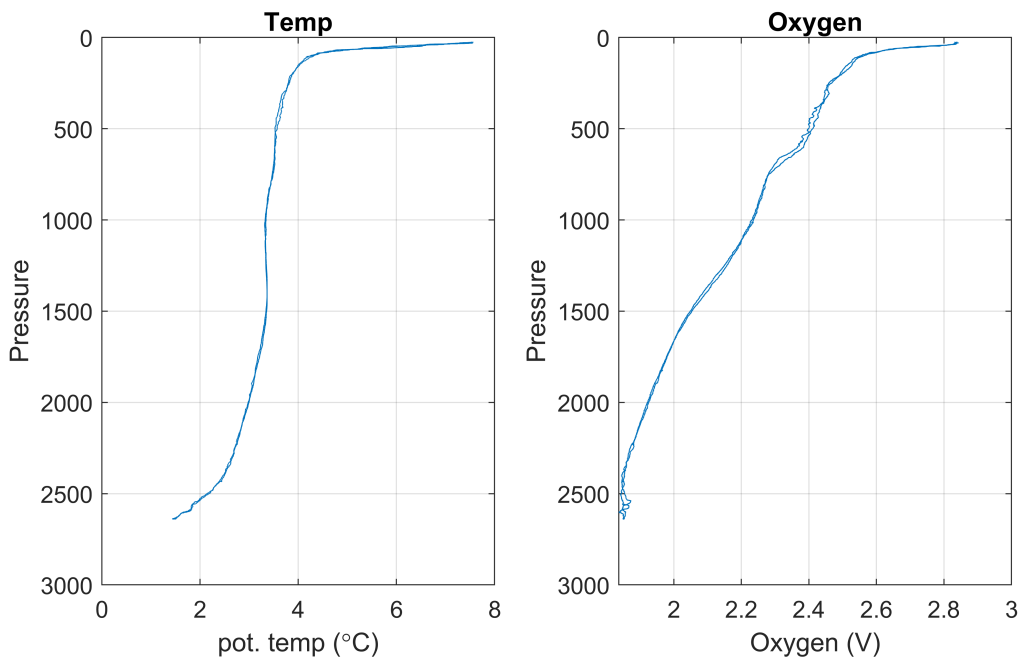


Figure B4: Potential temperature ($^{\circ}\text{C}$, left) and oxygen (voltages, right) processed with a default hysteresis correction and without an oxygen sensor time lag correction for Cast 21 on AR69-01.

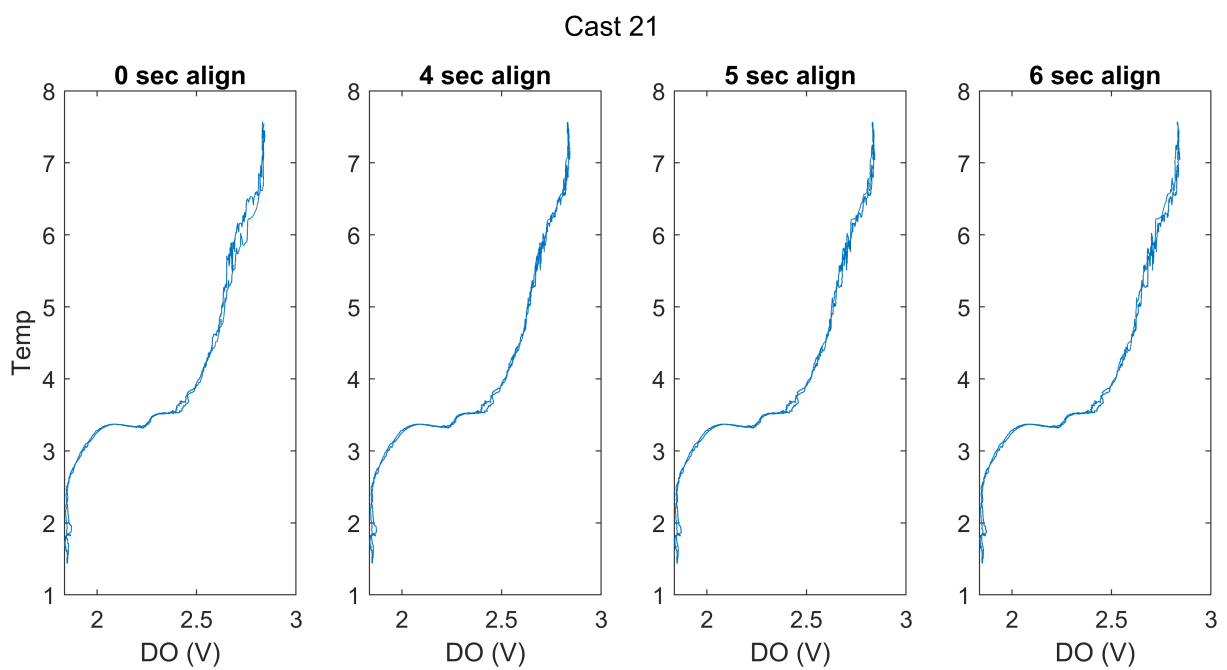


Figure B5: Oxygen (voltages) processed with a default hysteresis correction and shown in potential temperature ($^{\circ}\text{C}$) space with an oxygen sensor time lag correction relative to the pressure sensor from left to right of 0, 4, 5, and 6 seconds. A time lag correction of 4 seconds (second panel) was found to align upcast and downcast oxygen values in temperature space.

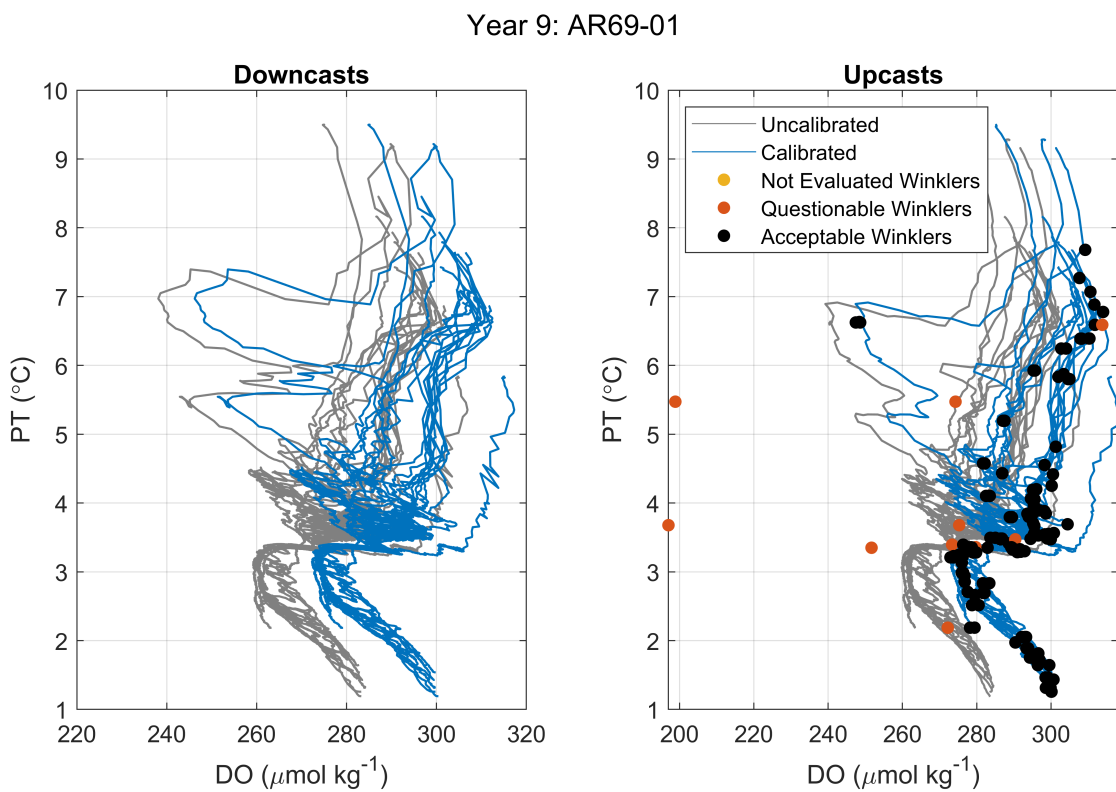


Figure B6: Factory calibrated (gray) and in-situ calibrated (blue) dissolved oxygen concentrations ($\mu\text{mol}/\text{kg}$) as a function of potential temperature ($^{\circ}\text{C}$) for downcasts (left panel) and upcasts (right panel). For upcasts, Winkler-measured oxygen concentrations ($\mu\text{mol}/\text{kg}$) are shown in circles with model-determined outliers indicated by red circles.